Separation and Purification Technology 247 (2020) 116947

Contents lists available at ScienceDirect

Separation and Purification Technology

journal homepage: www.elsevier.com/locate/seppur

Applications of metal-organic framework based membranes in water purification: A review

Byung-Moon Jun[a], Yasir A.J. Al-Hamadani[b], Ahjeong Son[c], Chang Min Park[d], Min Jang[e], Am Jang[f], Nam Chan Kim[e,*], Yeomin Yoon[a,*]

[a] Department of Civil and Environmental Engineering, University of South Carolina, Columbia, 300 Main Street, SC 29208, USA
[b] Directorate of Construction and Building, Ministry of Higher Education and Scientific Research of Iraq, 52 Street, Al-Rusafa, Baghdad 00964, Iraq
[c] Department of Environmental Science and Engineering, Ewha Womans University, 52 Ewhayeodae-gil, Seodaemun-gu, Seoul 03760, Republic of Korea
[d] Department of Environmental Engineering, Kyungpook National University, 80 Daehak-ro, Buk-gu, Daegu 41566, Republic of Korea
[e] Department of Environmental Engineering, Kwangwoon University, 447-1 Wolgye-Dong Nowon-Gu, Seoul, Republic of Korea
[f] School of Civil and Architecture Engineering, Sungkyunkwan University, 2066 Seobu-ro, Jangan-16 Gu, Suwon, Gyeonggi-do 440-746, Republic of Korea

ARTICLE INFO

Keywords:
Metal-organic frameworks
Membrane
Water treatment
Wastewater treatment

ABSTRACT

Metal-organic frameworks (MOFs) have attracted a great deal of attention due to their flexibility and various potential applications. MOF-based membranes have been widely applied in forward-osmosis (FO), reverse-osmosis (RO), nanofiltration (NF), and ultrafiltration (UF) processes. While a few recent studies have reviewed the applications of MOF-based membranes in water purification, a systematic understanding is still necessary to evaluate the transport mechanisms of various compounds by different MOF-based membranes under various operating and water-quality conditions. Here, we present a comprehensive literature review of recent findings and suggest future research trends by identifying insufficiencies of current knowledge, focusing on the performance of MOF-based membranes in water purification, as the transport of inorganic and organic compounds by MOF-based membranes is highly influenced by the different properties of compounds in addition to water-chemistry conditions and membrane properties. This study focused on several main parameters such as methods for synthesis of MOF-based membranes, membrane properties, and the physicochemical properties of various compounds, which affect the transport of compounds during MOF-based FO/RO/NF/UF membrane filtration. In addition, we provide the continuing challenges and areas of future study in this field.

1. Introduction

Many areas of the world have experienced both urbanization and industrialization to an extraordinary degree over the last 50 years [1]. As natural resources play important roles in urbanization and industrialization, worldwide material consumption has increased rapidly and almost doubled between 1980 and 2009 [2]. In particular, water use has risen with the increases in population associated with urbanization and industrialization, which have also placed alarming pressure on water resources worldwide [3]. In addition, water quality has decreased over the last few decades, mostly due to human activities and poor use of natural water resources [4]. Many previous studies have shown that contaminants of emerging concern, such as endocrine disruptors, pharmaceuticals, and personal care products, can be detected at very low concentrations (< 1 μg/L) in wastewater effluents and drinking water around the world [5–7]. Therefore, it is essential to develop cost-effective treatment methods for water purification.

Various conventional and advanced treatment processes have been widely used in water-treatment plants for the removal of conventional and emerging contaminants, including coagulation-flocculation-sedimentation-filtration [8,9], ozonation [9], adsorption [10,11], membranes [12,13], and ultrasonication [14,15]. Among these processes, membrane filtration is relatively reliable, flexible, and predictable, and provides important advantages in water and wastewater treatment applications [16]. However, the presence of various inorganic and organic compounds in water affects membrane fouling, selectivity, and flux. To enhance membrane performance, membranes that are blended/coated with various emerging (nano)materials—e.g., carbon nanotubes [17], graphene oxides [18,19], MXenes [20,21], metal–organic frameworks (MOFs) [22,23])—have been developed, which have attracted interest in the water industry due to their enhanced selectivity, hydrophilicity, and fouling resistance.

* Corresponding authors.
E-mail addresses: kimnc@kw.ac.kr (N.C. Kim), yoony@cec.sc.edu (Y. Yoon).

https://doi.org/10.1016/j.seppur.2020.116947
Received 9 January 2020; Accepted 23 March 2020
Available online 28 April 2020
1383-5866/

Among these emerging materials, MOFs (organic–inorganic hybrid microporous crystalline materials) have attracted a great deal of attention worldwide due to their flexibility and various potential applications [24]. In particular, MOFs have exceptional characteristics because: (i) MOFs have high tunable porosities and accessible large surface areas [25], and (ii) MOFs have a high capacity to combine particular species/functionalities easily without changing the framework topology [26]. A number of recent studies have demonstrated different environmental applications of various MOFs in adsorption [27,28], catalysis [29], and membranes [30,31]. With regard to membrane applications, MOFs have been widely applied in forward osmosis (FO, MOF thin-film-based porous matrix membranes [32], UiO-66 thin-film nanocomposite (TFN) membranes [33], and MOF-cellulose acetate triacetate membranes [34]), reverse osmosis (RO, TFN membranes filled with UiO-66 and MIL-125 [35], TFN membranes doped with MIL-101(Cr) nanoparticles [36], and polyamide@NH_2-MIL-88B nanocomposite membranes [37]), nanofiltration (NF, Zr-based MOF-808 nanofibrous membranes [38], UiO-66-incorporated TFN membranes [39], and TFN membranes with the minimum amount of MOF (MIL-101(Cr)) [40], and MIL-53(Al) nanocomposite membranes [41]), and ultrafiltration (UF, UiO-66@graphene oxides/polyether sulfone membrane [42], MIL-101(Cr)-laccase-polyacrylonitrile membranes [43], and 67-MIL-polyvinylidene fluoride membranes [44]).

Several recent studies have reviewed the applications of MOF-based membranes in water purification [3,45,46]. While these studies focused on water desalination in different membrane processes and also offered comprehensive summary of the applications of MOF-based membranes, further studies are necessary to obtain a systematic understanding to evaluate the transport mechanisms of various conventional and emerging contaminants under various membrane operating and water-quality conditions in different membrane processes. Thus, a comprehensive review of the performance of MOF-based membranes in water purification is significant, because the removal of both inorganic and organic compounds by MOF-based membranes is highly affected by the different properties of compounds in addition to water-chemistry conditions and membrane properties. In this review, we first provided a brief introduction to the different types of MOFs that are incorporated with FO, RO, NF, and UF membranes. Then, we focused on the preparation techniques and treatment performance of various MOF-based membranes. In particular, this study focused on several main parameters, i.e., methods of synthesis of MOF-based membranes, membrane properties, and the physicochemical properties of various compounds, which affect the transport of various inorganic and organic compounds and water permeance during MOF-based membrane filtration.

2. Preparation techniques and treatment performance of various MOF-based membranes

Since the introduction of MOFs to membranes in various industries to enhance their general performance, numerous techniques for preparation of MOF-based membranes have been developed, including TFN [33], (porous) mixed matrix [47], the solvothermal method [48], the electrodeposition method [49], and vacuum filtration [50]. These techniques have been used to improve the design of MOF-based membranes for liquid separation, particularly in the area of desalination using capacitive deionization [51], adsorption desalination [52], and membrane distillation [53], as well as FO, RO, NF, and UF. Fig. 1 illustrates several design methods for MOF-based membranes in liquid separation: the in situ preparative route, the blending method, and the interfacial polymerization process. Appropriate design of MOF-based membrane fabrication approaches is critical to achieving accurate and rapid water purification. The performance of MOF-based FO, RO, NF, and UF membranes in water treatment depends significantly on the development of preparation methods, which critically affect the configuration of MOF-based membranes and their strength and removal effectiveness [54].

2.1. FO membranes

2.1.1. Synthesis methods

While the principles were confirmed in the 1960s, the FO process has recently been widely adopted for different applications, particularly seawater desalination [55]. Scientists and engineers have searched for new techniques for the fabrication of FO membranes for use in the water industry. While various porous matrix membranes (PMMs) have been used for NF [56] and UF [57] membranes, the use of PMM for FO-TFN membranes is somewhat uncommon due to their similarity in structure to porous asymmetric membranes [58]. To avoid this limitation, for FO applications it is necessary to create a highly stable, active, and dense layer on the top surface of the membrane. Arjmandi et al. fabricated a thin-film PMM combined with magnetic water-unstable MOFs ((magnetic) ZnO@MOF-5) by adjusting the traditional dense film-casting technique, which showed a substantial impact on the performance of the FO process [32]. In a separate study, a TFN membrane with a well-suited 2D MOF (copper 1,4-benzenedicarboxylate) nanofiller in a polyamide active layer during interfacial polymerization was fabricated to enhance water flux and antifouling ability without reducing the selectivity for FO applications [59]. Fabrication of Cu-1,4-benzenedicarboxylate nanosheet/polyamide TFN membranes based on reaction and post-treatment procedures was comparable to that of thin-film composite membranes, except that a Cu-1,4-benzenedicarboxylate nanosheet was added at various concentrations of 0.03–0.15 wt/v% trimesoyl chloride/*n*-hexane solution before interfacial polymerization.

To improve the FO performance, it is critical to control the internal concentration polarization. Lee et al. utilized MOFs as a detachable filler to fabricate MOF-based PMMs to enhance the mass transfer efficiency in FO support substrates by controlling the internal concentration polarization (i.e., smaller structural parameter value) [47]. The structural parameter is commonly used to determine the severity of internal concentration polarization. MOF-based porous matrix substrates with three different types of MOFs were prepared by phase inversion with MOF particles mixed in a polyacrylonitrile doping solution: aluminum-based MIL-53, copper-based Cu-BTC, and iron-based MIL-100 MOF particles. The order of FO membrane water flux with these MOFs (PMM- Cu-BTC > PMM- MIL-53 > PMM- MIL-100) corresponded to the reverse order of the MOF structural parameter (PMM-Cu-BTC < PMM-MIL-53 < PMM-MIL-100). The improved FO performance was the result of the development of relatively large macropores inside the PMMs, which enhanced the mass (water/solute) transfer effectiveness inside the PMM substrate.

Liu et al. developed a simple solution casting method followed by solvent evaporation to fabricate self-standing dense and homogeneous UiO-66 nanocomposite thin films (approximately 400 nm) incorporated into polysulfone with sulfonic functional groups [33]. It has been widely reported that interfacial binding with polymers is enhanced in the presence of UiO-66 in different noncovalent bonding forms by strengthening or post-synthesis swapping [60]. In particular, the development of interfacial binding between UiO-66 and the sulfonated polysulfone in thin films can occur in situ during the thin-film deposition process. The improved interfacial compatibility between the nanosized zirconium-based MOF (UiO-66) and sulfonated polysulfone additives decreases the conformational elasticity of the MOFs and polymer backbones, enhancing the structural properties and mechanical strength of thin films [33]. Fig. 2 illustrates the general scheme of fabrication of MOF-based nanofilms: (i) inter- and intramolecular hydrogen bonding occurs during the development of sulfonic polysulfone (*i.e.*, the sulfonic groups of ionic polymer binder) matrix thin film (Fig. 2a), which enables greater water permeance in osmotic pressure-driven processes [61]; (ii) UiO-66 was hypothesized to be well mixed with sulfonic polysulfone binder, thus producing very solid MOF-polymer binding for mixed matrix thin films (Fig. 2b); (iii) several synergistic effects are expected with self-standing thin films having microporous structures (Fig. 2c)—UiO-66 with a pore size of

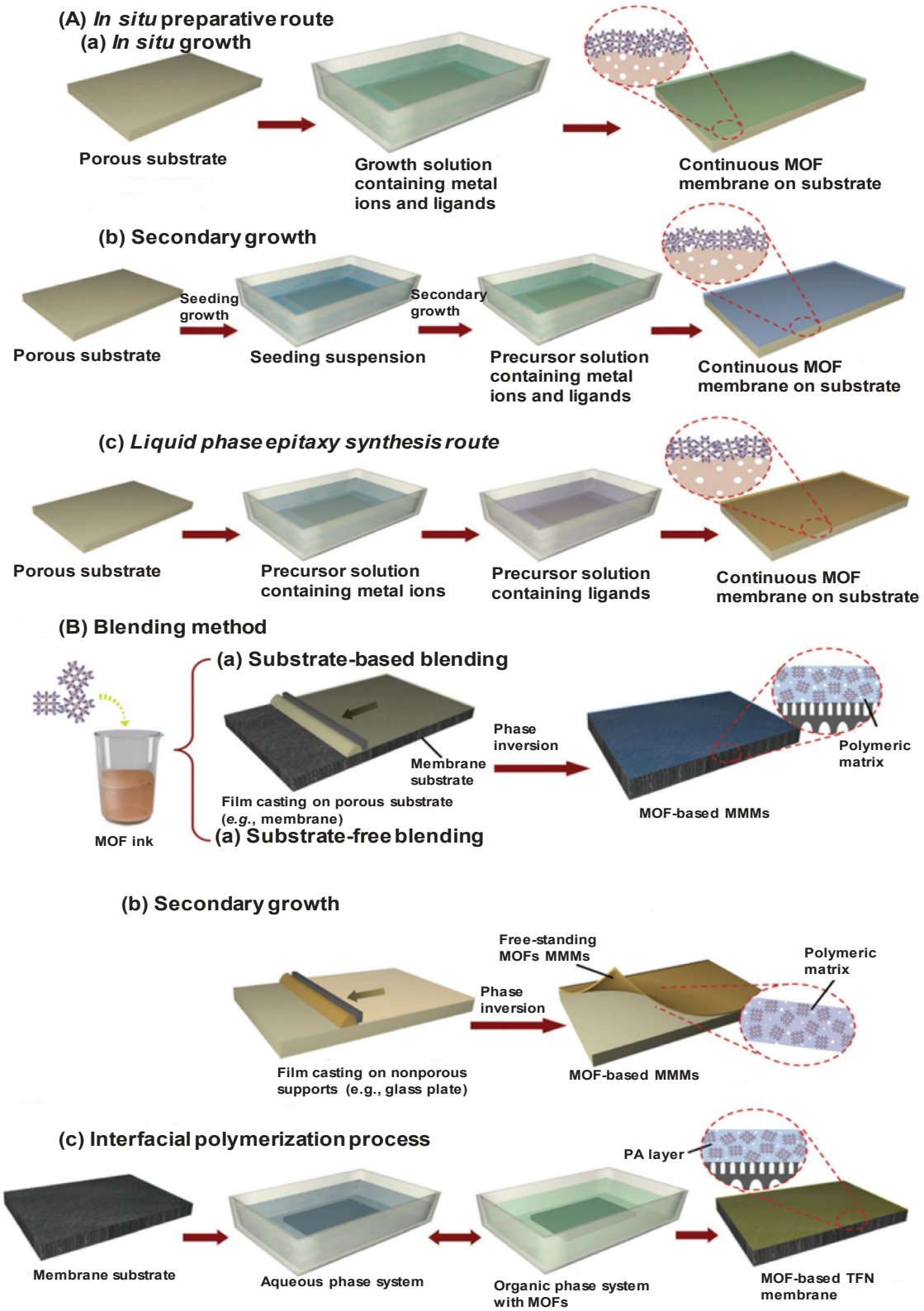

Fig. 1. Schematic illustration of design strategies for MOF-based membranes in liquid separation: (A) in situ preparative route; (B) blending method; (C) interfacial polymerization process [54].

approximately 0.6 nm readily allows passage of water molecules (approximately 0.28 nm), while hydrated ions (0.66–1.05 nm) are blocked. In addition, mixed matrix thin films could be beneficial to reduce internal concentration polarization and enhance the water flux in the FO process due to their supportive free symmetric configuration [33].

2.1.2. Membrane properties

FO is a process in which solvent/water passes through a semi-permeable membrane utilizing a difference in osmotic pressure produced by concentrated draw solution [13]. During the FO membrane process, the transport of solute is significantly influenced by membrane

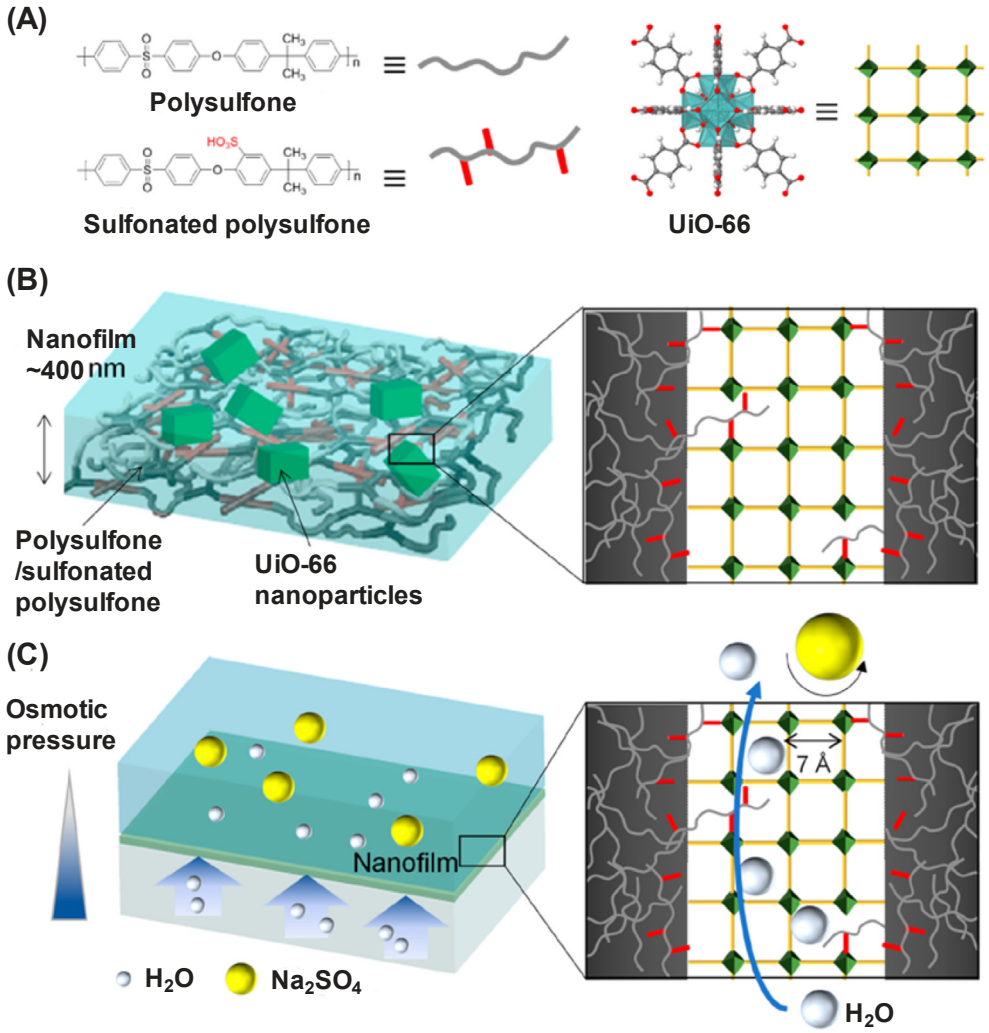

Fig. 2. General scheme of design of the MOF-based nanofilms. (A) Chemical formula of polymers, including polysulfone, sulfonated polysulfone, and an MOF, UiO-66. (B) Schematic diagram of mixed matrix nanofilm comprising UiO-66 nanoparticles and sulfonated polysulfone /polysulfone polymer chains; (right) the local binding interactions between the UiO-66 framework and the sulfonated polysulfone polymer chains. (C) Schematic diagram of separation performance with the free-standing mixed matrix nanofilm in FO; (right) the sub-nanometer pores within UiO-66 framework that act as water pathways and ion sieves for Na_2SO_4 [33].

properties and operating conditions. Dai et al. reported that the performance of porous MOF (Cu-1,4-benzenedicarboxylate) nanosheet/polyamide TFN membranes varied significantly depending on Cu-1,4-benzenedicarboxylate nanosheet dosages (0.03–0.12 wt/v%) for FO applications [59]. It is obvious that TFN membranes combined with Cu-1,4-benzenedicarboxylate nanosheets show greater water flux (approximately 22–50 L/m^2·h) and considerably less specific reverse solute flux (approximately 0.12–0.13 g/L) than the virgin thin-film composite membrane (approximately18-32 L/m^2·h and 0.25–0.27 g/L, respectively) in both active-layer-feed solution and active-layer-draw solution modes. As lower specific reverse solute flux indicates greater FO selectivity [62], the Cu-1,4-benzenedicarboxylate nanosheet TFN membrane showed an almost 50% decrease based on specific reverse solute flux compared to the virgin thin-film composite membrane in both operation modes, indicating substantial improvement of selectivity after Cu-1,4-benzenedicarboxylate nanosheet combination. In addition, the Cu-1,4-benzenedicarboxylate nanosheet TFN membrane showed approximately 60% greater water permeance and 25% lower salt permeability than the virgin thin-film composite membrane, which may be explained by the following reasons: (i) Cu-1,4-benzenedicarboxylate nanosheet has a pore size of 0.52 nm [63] that is greater than that of H_2O molecules (0.26 nm), which may provide extra channels for solvent transport. In addition to traditional solution-diffusion, the formerly ignored uniform pores on the polyamide layer surface may enhance water transport in FO processes along with convection and steric exclusion [64]. (ii) Incorporation of the Cu-1,4-benzenedicarboxylate nanosheet into the polyamide layer enhances the surface hydrophilicity of the membranes, which is advantageous to enhance water transport [65]. The contact angle of Cu-1,4-benzenedicarboxylate nanosheet TFN membrane was reduced by approximately 35% compared to the virgin TFC membrane [59] due to the presence of the Cu element and the COOH groups of the nanosheets [66], while no substantial changes were observed in roughness between the two membranes. (iii) The enhanced selectivity may also be due to size exclusion by the relatively small pores of the Cu-1,4-benzenedicarboxylate nanosheet compared to hydrated Cl^- (0.66 nm) and Na^+ (0.72 nm) ions [67].

The properties of UiO66-TFN membranes varied depending on the amount of UiO-66 loading, which significantly influenced both water adsorption and permeance [33]. In addition, the results of stretching and hydraulic bursting tests indicated outstanding mechanical properties of the MOF-based membranes compared to their virgin polymer counterparts·H_2O passage in microporous materials is governed by solution diffusion; the H_2O molecules are adsorbed in the extrinsic micropores (0.9–1.2 nm) and diffuse through the membrane pores. Therefore, the transport of adsorbed H_2O molecules is enhanced due to

weak binding of H_2O molecules with hydrophobic MOFs [68]. The UiO66-TFN membranes showed greater water permeance (0.52 L/m^2·h·bar) and retention performance for phenol red (> 99%) and Na_2SO_4 (94–96%) at an initial concentration of 20 mmol/L than their virgin polymer counterparts (water permeance, 0.026 L/m^2·h·bar; phenol red, 91%; Na_2SO_4, 73%) in both NF and FO processes [33].

During FO processes, water flux decreases and energy requirement increases in the presence of microorganisms due to their adhesion associated with proliferation and distribution on the membrane surface [69]. Firouzjaei et al. fabricated a TFN membrane that incorporated a graphene oxide (GOs)-Ag based MOF (GOs-Ag-MOF) to improve antibiofouling properties and water permeability in the presence of *Escherichia coli* and sodium alginate in FO processes [70]. The GOs-Ag-MOF TFN membrane showed approximately 96% *E. coli* growth inhibition, which was much higher than thin-film composites (2%), GOs (66%), and Ag-MOF TFN membranes. These findings indicated that the GOs-Ag-MOF membrane had greater potential antimicrobial activity than did individual Ag-MOF and GOs nanomaterials [71], which could contribute significantly to the biological fouling and fouling resistance of the membrane as well as membrane surface roughness, surface charge, and hydrophobicity. The GOs-Ag-MOF TFN membrane had somewhat high surface roughness, with a relatively high negative surface charge and low hydrophobicity, which resulted in high fouling resistance during the FO processes [70]. Fig. 3 shows several key parameters, including contact angle, zeta potential, and surface roughness, which contribute to the antibiofouling properties of the TFC, GOs TFN, GOs-Ag-MOF, and Ag-MOF TFN membranes.

2.1.3. Permeance and removal

To evaluate the performance of FO membranes, water permeance, salt permeability, water flux, and specific reverse solute flux have typically been compared as essential transport parameters. FO membrane selectivity is commonly evaluated based on the salt permeability/water permeance ratio; in general a low salt permeability/water permeance ratio indicates high selectivity, which is desirable in the FO process [72]. In particular, the specific reverse solute flux is a significant parameter to evaluate the amount of salt lost during the FO process. A novel integral thin-film PMM in the FO process showed outstanding water flux of approximately 100, 120, and 140 L/m^2·h for orange juice concentration, Caspian seawater desalination, and deionized water as feed solutions, respectively [32]. The results indicated that there is a clear linear relationship between the salt permeability/water permeance and the specific reverse solute flux ratio. In addition, the water flux was much higher for thin-film PMMs than for pure polyethersulfone membranes in both active-layer-draw solution and active-layer-feed solution modes. Regardless of the orientation mode, the water flux increased with increasing draw solution concentrations from 0.5 to 2.0 M (NaCl) due to the higher osmotic pressure associated with increased internal concentration polarization produced across the FO membranes [32]. In a separate study, Cu-1,4-benzenedicarboxylate nanosheet TFN membranes with municipal wastewater exhibited greater water flux and obvious antifouling behavior compared to the virgin thin-film composite membrane [59]. These findings imply that use of Cu-1,4-benzenedicarboxylate nanosheet combined with TFN membranes may be very useful in FO processes in both seawater desalination and wastewater treatment.

The FO water flux of an MOF-based membrane (PMM-C300) was significantly influenced by different draw-solution ($MgCl_2$, 0.1–3.0 M) and feed-solution (NaCl, 0–100 mM) concentrations [47]. In all membrane orientations, greater draw-solution concentrations resulted in greater FO water flux for the MOF-based PMM, presumably due to the higher osmotic pressure produced across the membrane. In particular, in active layer-draw-solution orientation, the FO water flux of PMM-C300 (34–133 L/m^2·h) increased with increasing draw-solution concentrations (0.1–3.0 M $MgCl_2$) due to the increase in osmotic driving force [73]. In a separate study, a MOF (UiO-66)-TFN membrane with 0.1 wt% particle loading significantly improved water permeability (approximately 50%) compared to the pristine thin-film composite membrane and showed a very high salt-rejection rate (approximately 95%) with 1000 mg/L NaCl as the feed solution [74]. In addition, the greatest water fluxes of 51.3 and 27 L/m^2·h for the MOF-TFN membrane were achieved in the pressure retarded osmosis mode and FO mode, respectively. Pang et al. fabricated sandwich antimicrobial membranes incorporating MOF (UiO-66)-GOs, which showed 270% higher water flux (29.2 L/m^2·h) and 84% lower reverse solution diffusion (12.9 L/m^2·h) than the virgin GO membrane [75]. Fig. 4 shows a

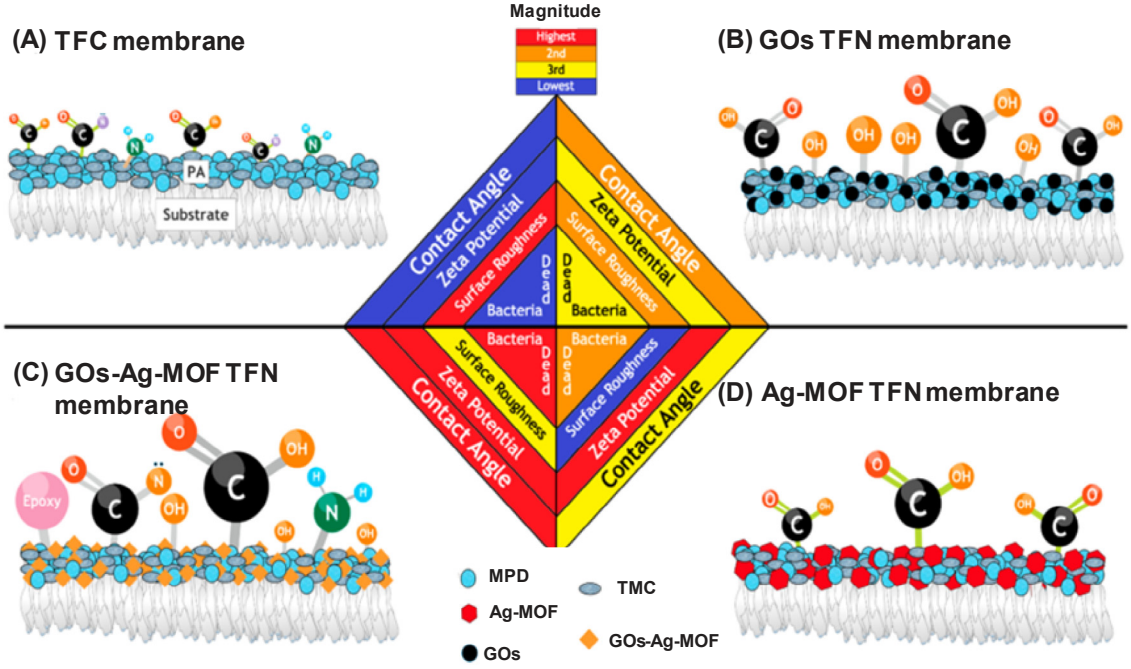

Fig. 3. Parameters contributing to anti-biofouling and antifouling properties of the membranes: (a) Thin-film composite, (b) GOs TFN, (c) GO-Ag-MOF TFN, and (d) Ag-MOF TFN membrane (MPD = 1,3-phenylendiamine; TMC = trimesoylchloride) [70].

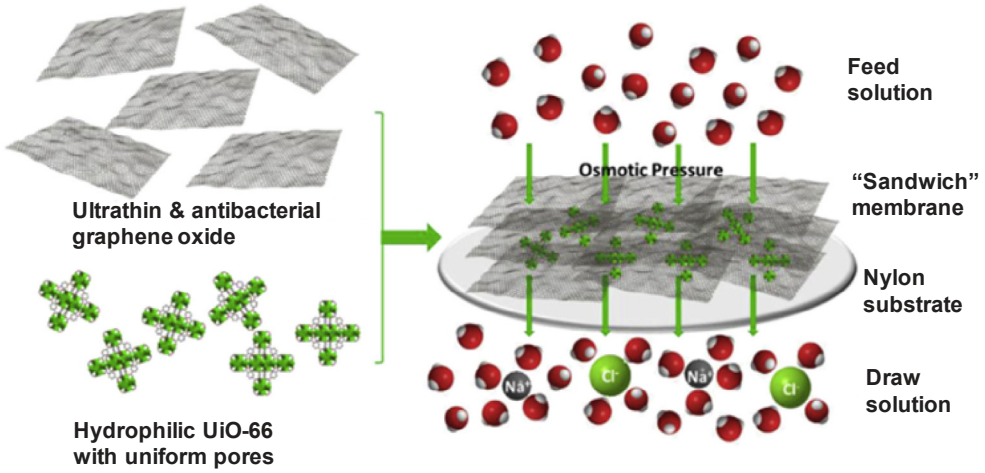

Fig. 4. Schematic diagram of UiO-66/GO "sandwich" membrane for FO process [75].

schematic diagram of the MOF-GO membrane, indicating that the layered GOs play an important role in forming a very thin membrane on the Nylon substrate, while the MOFs act as microporous filler combined among the GO layers. In a separate study, a ZIF-8@polydopamine TFN membrane exhibited high degrees of heavy metal removal (Pb^{2+}, Cu^{2+}, and Ni^{2+} > 96%) in FO mode, while the MOF membrane still had greater water flux (20.8 L/m^2·h) than the pristine membrane (12.8 L/m^2·h) without selectivity reduction (salt permeability/water permeance ratio = 0.25 and 0.20 g/L, respectively) [76].

2.2. RO membranes

2.2.1. Synthesis methods

As RO membranes have been widely adopted in water treatment and desalination, various commercial RO membranes have been optimized for high water flux and solute removal, particularly by modifying a thin-film composite structure on a very thin polyamide selective layer [77]. Duan et al. fabricated polyamide TFN RO membranes effectively incorporating thermally stable and hydrophobic zeolitic imidazolate framework-8 (ZIF-8) for water desalination [78]. The possible benefits of ZIF-8 over conventional hydrophilic zeolite used in TFNs include theoretically higher water passage within the MOF and enhanced compatibility with the polyamide matrix. In a separate study, interfacial polymerization between *m*-phenylenediamine and trimesoyl chloride was formed to fabricate TFN membranes incorporating two different MOFs (UiO-66 and MIL-125, approximately 100 nm) into polysulfone thin-film composite membranes with various loadings (0–0.3%) [35]. Overall, the UiO-66- and MIL-125-modified TFN membranes exhibited improved NaCl rejection and water flux, which still varied depending on the nanoparticle weight ratios. The same method was employed to fabricate TFN RO membranes incorporating HKUST-1 ($Cu_3(BCT_2)$) [79]. The determined active-layer thickness of the HKUST-1/RO membrane (29 nm) was much smaller than that of a commercial RO membrane (200 nm), which exhibited enhanced water flux and antifouling compared to the pristine thin-film composite RO membrane with a polysulfone support layer, without changing the $NaHCO_3$ rejection behavior.

Reversible accumulation–fragmentation chain transfer polymerization as an active thin surface layer at the commercially available RO membrane support was employed to fabricate an antimicrobial multilayer membrane incorporating phosphonium-conjugated GO-anchored Cu- and trimesic acid-based MOF (*p*GO-Cu-MOF) [80]. These modified *p*GO-Cu-MOF membranes rapidly inactivated bacteria with 7-log reductions in numbers of gram-positive and gram-negative bacteria, and also showed severe and targeted reactions in terms of reactive oxygen species production. Wang et al. fabricated unique polyamide nanocomposite RO membranes incorporating amino-functionalized MIL type MOFs (NH_2_MIL-88B) for water purification [37]. The RO support layer was modified by developing an interlayer of the MOF nanoparticles followed by a polysulfone layer coated on the MOF interlayer, which has a lower degree of cross-linking, is thinner, and has low hydrophobicity compared to the original polyamide RO membranes. A separate study indicated that highly water-permeable TFN membranes incorporating stable and hydrophilic porous MIL-101(Cr) were successfully fabricated on a polysulfone support with a dense selective polyamide layer for RO applications [36]. Highly permeable direct water channels formed in the presence of hydrostable porous MOF nanoparticles in the polyamide layer, which increased membrane water flux by allowing H_2O molecules to pass through rapidly.

2.2.2. Membrane properties

The RO water flux and NaCl rejection by ZIF-8/TFN polyamide membranes were significantly influenced by the MOF loading rates [78]. Incorporation of different amounts of MOFs (ZIF-8, 0.05% and 0.4%) enhanced the water flux by approximately 90% and 160%, respectively, compared to pristine polyamide membranes, while similar findings have also been reported with silicalite-1 [81] and carbon nanotubes [82]. In addition, NaCl rejection increased slightly with increasing MOF loading (98.2% with no ZIF-8 and 98.7% with 0.1% ZIF-8) and then decreased slightly with further increases in MOF loading (98.5% with 0.4% ZIF-8). In theory, while the ZIF-8 pore size of 0.34 nm is small enough to remove > 99% of hydrated Na^+ and Cl^- in water, the inconsistent findings were presumably due to polyamide structure adjustment associated with potential holes between ZIF-8 and polyamide [78]. NaCl rejection is also significantly influenced by operating conditions, such as flow rate, as concentration polarization increases with increasing water flux.

Gupta et al. reported a molecular simulation study in which the rejection of NaCl by various ZIF membranes was significantly affected by their functional groups influencing membrane polarity, charge, and hydrophobicity, as well as pore size [46]. Overall, the water flux with NaCl by ZIF membranes (27–710 L/m^2·h·bar) was found to be one to two orders of magnitude greater than those of commercial RO membranes. Fig. 5 illustrates water desalination through a ZIF membrane with a NaCl concentration of 0.5 M mimicking the salt concentration of seawater. Another molecular simulation study indicated that the water flux through a ZIF-8 membrane was significantly improved [83], although there were several limitations for the simulation study: (i) An inflexible model was used for the ZIF-8 membrane, which would make it difficult for Na^+ and Cl^- ions to pass through the small pores; (ii) due to computational resources, the simulation period was too short compared to a real membrane filtration process; (iii) greater external

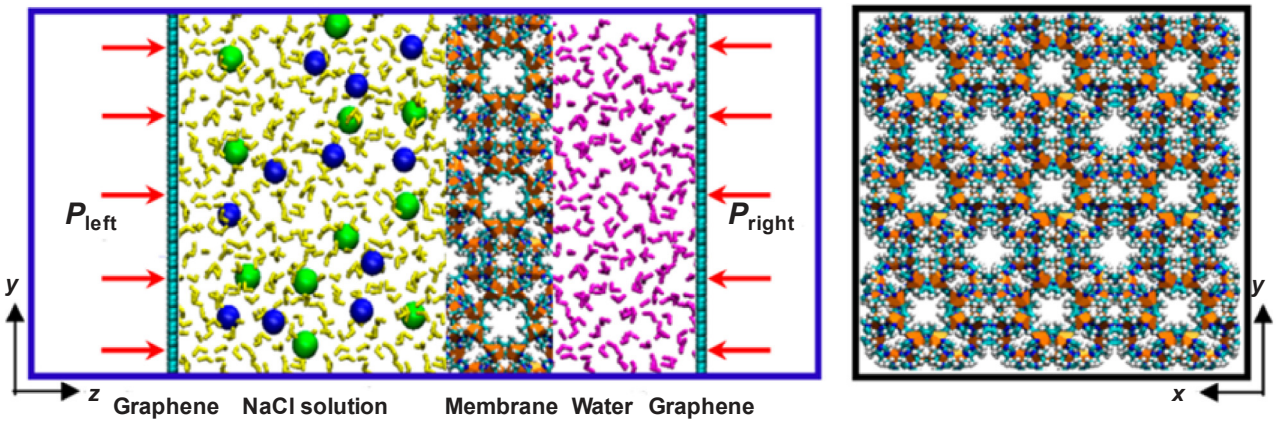

Fig. 5. Simulation system for water desalination through a ZIF membrane [46]. An aqueous NaCl solution with 0.5 M NaCl and pure water bath are on the left and right chambers of the membrane, respectively. Two graphene plates in the two chambers are exerted under hydraulic pressures P_{left} and P_{right}, respectively. Zn: orange, N: blue, C: cyan, H: white; graphene: cyan; Na^+: blue, Cl^-: green; water molecules in the left and right chambers: yellow and magenta. (For interpretation of the references to colour in this figure legend, the reader is referred to the web version of this article.)

pressures compared to theoretical scenarios were employed to simulate the apparent RO process on a nanosecond scale; and (iv) the simulation was conducted with the assumption of a very thin ZIF-8 membrane due to computational resource limitations, which may not be comparable to an actual membrane [83].

Park et al. investigated the performance of HKUST-1/RO membrane fouling with bovine serum albumin (100 mg/L) [79]. The HKUST-1/RO membrane exhibited a non-significant decrease in flux (< 5%), while the pristine thin-film composite RO membrane showed much faster membrane flux decline (approximately 40%) with a filtration period of 8 h, indicating that the MOF/RO membrane showed exceptional anti-fouling behavior against bovine serum albumin without altering the salt-removal capacity. Based on the contact angle and results of atomic force microscopy analyses, the MOF/RO membrane became more hydrophilic and smoother than the pristine RO membrane, which resulted in reduced membrane fouling due to the adsorption of organic compounds [79]. In a separate study, a modified (multilayered) *p*GO-Cu-MOF membrane that included an active layer, RO support, and interlayer *p*GO-Cu-MOF showed outstanding antibacterial behavior, presumably because of the obvious antibacterial effects of the phosphonium cations and ammonium ions [80]. While the multilayered MOF membrane showed approximately 2–5% higher levels of monovalent and divalent mixed salts (NaCl, $MgCl_2$, and $Ca(NO_3)_2$) than the pristine RO membrane, approximately 15% lower water flux was observed for the multilayered MOF membrane due to the enhanced resistance of H_2O molecules passing through the interlayered membrane structure. In addition, salt rejection was somewhat affected by the initial concentrations: 99.9%, 98.6%, 97.9%, and 96.8% at 250, 400, 1000, and 2000 mg/L, respectively. The rejection mechanisms vary depending on the layer: (i) Electrostatic repulsion governs the rejection of cations by the positively charged active layer, and (ii) steric exclusion efficiency by the *p*GO-Cu-MOF interlayer is higher than that by the pristine RO membrane support layer [84]. Fig. 6 shows the particular roles of each layer concerning the comprehensive decontamination of water by the multilayered MOF membrane.

2.2.3. Flux and removal

The water flux and NaCl rejection by membranes incorporating MIL-125 and UiO-66 were evaluated under MOF loading conditions of 0%, 0.05%, 0.1%, 0.2%, 0.3%, and 0.5% [35]. For MIL-125 membranes, the highest NaCl rejection (98.7%) and water flux (89 $L/m^2{\cdot}h$) were obtained at loading rates of 0.1% and 0.5%, respectively, while for UiO-66 membranes, the optimal loading was 0.05% for salt rejection (99.2%) and 0.15% for water flux (75 $L/m^2{\cdot}h$). Relatively low loading of UiO-66 enhanced salt rejection due to the larger pore size (0.6 nm) than H_2O (0.28 nm), but smaller than the hydrated Na^+ (0.72 nm) and Cl^- (0.66 nm) ions [85]. However, addition of excessive amounts of nanoparticles decreased both NaCl rejection and water flux, presumably due to cracks associated with the accumulation of nanoparticles in the membrane structure [35]. In particular, particle accumulation may produce small micrometer-scale holes between particle blocks, which permit the water to readily transfer through. The overlap of low hydrophilic linkers caused by particle accumulation may also reduce water flux through the membrane [86]. In another study, the performance of an HKUST-1/RO membrane in terms of water flux and $NaHCO_3$ rejection was compared with that of a pristine RO membrane with a polysulfone support layer [79]. The water flux of the pristine RO membrane was 36.5 $L/m^2{\cdot}h$ with $NaHCO_3$ rejection of 94%, while the water flux of the MOF-RO membrane was enhanced by 33% (36.5 $L/m^2{\cdot}h$) with the incorporation of acid HKUST-1, with salt rejection of 96%. These findings may be explained by the increased hydrophilicity and porosity of the polysulfone support layer that decreases the *m*-phenylene diamine diffusion rate in water [87].

An NH_2_MIL-88B RO membrane enhanced water flux (35.8 $L/m^2{\cdot}h$) compared to a thin-film composite membrane (23.5 $L/m^2{\cdot}h$), while both membranes showed somewhat similar phenol removal (91–92%) [37]. The difference in performance may be explained by surface modification with porous nanofillers (porous structure, content, and size) that influence the pore structure (size and porosity) of the polysulfone nanocomposite layer (degree of polyamide crosslinking and thickness). In particular, the polysulfone nanocomposite layer can be modified in terms of porosity and pore size by having an optimized amount of porous nanofillers in the polysulfone, which enhance the performance during RO processing. Previous studies showed that polyamide TFN membranes with greater amounts of filler showed relatively low membrane selectivity due to filler aggregation associated with the uneven distribution of filler in the aqueous-organic phase [88]. In addition, a simple one-step interfacial polymerization method may allow fabrication of membranes through only one interfacial polymerization procedure, which is more beneficial than the two-step interfacial polymerization method in terms of water flux during membrane processing [37].

Highly stable TFN-MIL-101(Cr) membranes exhibit varying water permeance and NaCl rejection depending on the amount of MOF loading [36]. Water permeance (~2.1 $L/m^2{\cdot}h{\cdot}bar$) by a TFN-MIL-101(Cr) membrane containing 0.025 w/v% MOFs was enhanced by approximately 40% compared to a thin-film composite membrane (1.5 $L/m^2{\cdot}h{\cdot}bar$). Water permeance continued to increase with increasing MIL-101(Cr) MOFs (~3.0 $L/m^2{\cdot}h{\cdot}bar$ at 0.1 w/v%). As described previously, the hydrophilic porous MOF structure and the small

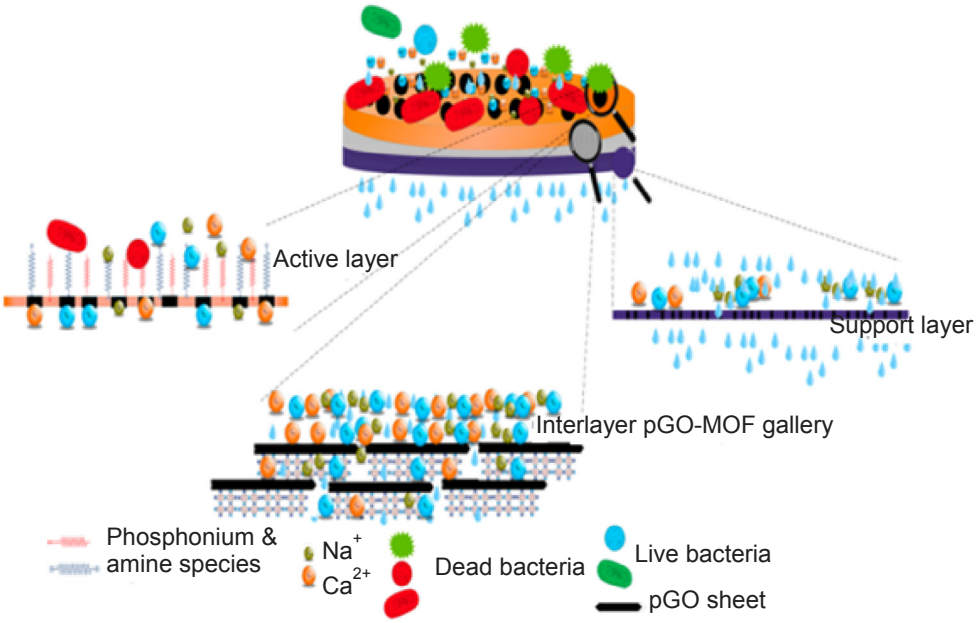

Fig. 6. Specific roles of each layer towards the complete decontamination of water by the multilayered MOF RO membrane [80].

degree of crosslinking of the polyamide structure contributed considerably to the improvement of water permeance, as the typical straight channels allow H_2O molecules to pass through. However, the NaCl rejection decreased from 99.5% to 93.5% with increasing MOF loading amount, presumably due to the inner nonselective voids of MOF nanoparticle aggregations, and interfacial defects between the polyamide and the aggregations [36].

2.3. NF membranes

2.3.1. Synthesis methods

Various NF membranes to separate inorganic and organic solutes from water or organic solvents are commercially available. Commercially available NF membranes are usually prepared with glassy and rubbery polymers (e.g., polydimethylsiloxane, polyamide, and polyimide), which are low cost, stable, and highly selective in organic solvents [89]. However, it is still challenging to fabricate high flux and selective polymeric membranes for application in water purification [90]. Cheng et al. examined the performance of ultrathin polyamide NF membranes incorporating MOFs for the removal of dyes and antibiotics [91]. To break the trade-off between membrane flux and selectivity, in particular, extra molecular transport channels were successfully created in the polyamide membranes combined with highly hydrostable UiO-66 nanoparticles with various functional surface structures. Efome et al. successfully fabricated a MOF (Zn-based MOF-808, $Zr_6O_4(OH)_4(COOH)_6(BTC)_2$) nanofibrous NF membrane with intrinsic hydrophilic polyacrylonitrile nanofibers prepared through co-electrospinning. The MOF nanofibrous membrane showed high removal of Cd^{2+}/Zn^{2+} and reusability of the membrane. The fiber size of the polyacrylonitrile with the MOF nanoparticles was considerably larger than the polyacrylonitrile without MOF loading, which increased the surface roughness. Different activation directions, such as "hydractivation" to expand membrane pores, as shown in Fig. 7, were verified to determine the capacities of this unsophisticated method.

The phase inversion method associated with immersion precipitation was employed to fabricate Zn-based MOF (MOF-5) incorporating polymeric membranes (polyethersulfone, cellulose acetate, and polyvinylidene fluoride) for the removal of heavy metals (Cu^{2+} and Co^{2+}) [92]. Fig. 8 shows a schematic of heavy metal removal from water by a MOF-5 NF membrane with polymer incorporation. He et al. synthesized stable MOF UiO-66 nanoparticles with various diameters (30, 100, and 500 nm) and fabricated TFN membranes incorporating UiO-66 MOFs into the selective cross-linked polyamide layer on the polyethersulfone substrate [39]. Various degrees of UiO-66 nanoparticle loading (0–1.25 wt%) were employed in the fabrication of MOF TFN membranes, which were used to evaluate the effects of nanoparticle size and loading on the removal of Se and As. In another study, amino-functionalized MOF (IFMOF-3)/GO composites were coated onto a stable polydopamine surface layer on a polysulfone substrate for Cu(II) removal [93]. The IRMOF-3/GO membrane showed high Cu(II) rejection (approximately 90%) and exceptional stability (33.3-hour filtration period) at a relatively high water flux of 31 $L/m^2 \cdot h$ at 0.7 MPa.

ZIF-8-based hollow nanocube TFN membranes incorporated into the polyamide layer were fabricated through an interfacial polymerization method [94]. Exceptional NF performance was obtained in terms of water permeance and salt rejection (NaCl and Na_2SO_4) due to the unique properties of the hollow nanocubes based on hydrophilicity, hollow configuration, and negative charge. Liu et al. fabricated stable MOF (HKUST-1)-reduced GO nanocomposite membranes incorporating polydopamine on a cellulose acetate support layer for organic dye removal [50]. Polydopamine with several functional groups, such as amine and catechol, provides outstanding reduction and stability characteristics [95]. The Langmuir–Schaefer method was used to fabricate TFN membranes incorporating hydrophilic MIL-101(Cr) between an ultrathin polyamide layer and a cross-linked asymmetric polyimide support layer [40]. Paseta et al. employed two different MOFs (ZIF-93 and HKUST-1) to fabricate polyamide-MOF bilayer TFN membranes for removal of pharmaceuticals via the interfacial synthesis and interfacial polymerization method for the MOF and polyamide layer, respectively [96]. A ZIF-8@GO NF membrane incorporating polyethyleneimine was fabricated on a tubular ceramic support via a vacuum-assisted assembly technique to improve organic solvent (methanol) NF performance for dye transport [97].

2.3.2. Membrane properties

Polyamide/UiO-66 NF membranes were fabricated to separate different dyes and an antibiotic (rose Bengal, thiazole yellow G, crystal violet, methyl orange, safranin O, and azithromycin) from various solvents, including methanol, ethanol, isopropanol, acetone, methyl ethyl ketone, and ethyl acetate [91]. While the pure water permeance

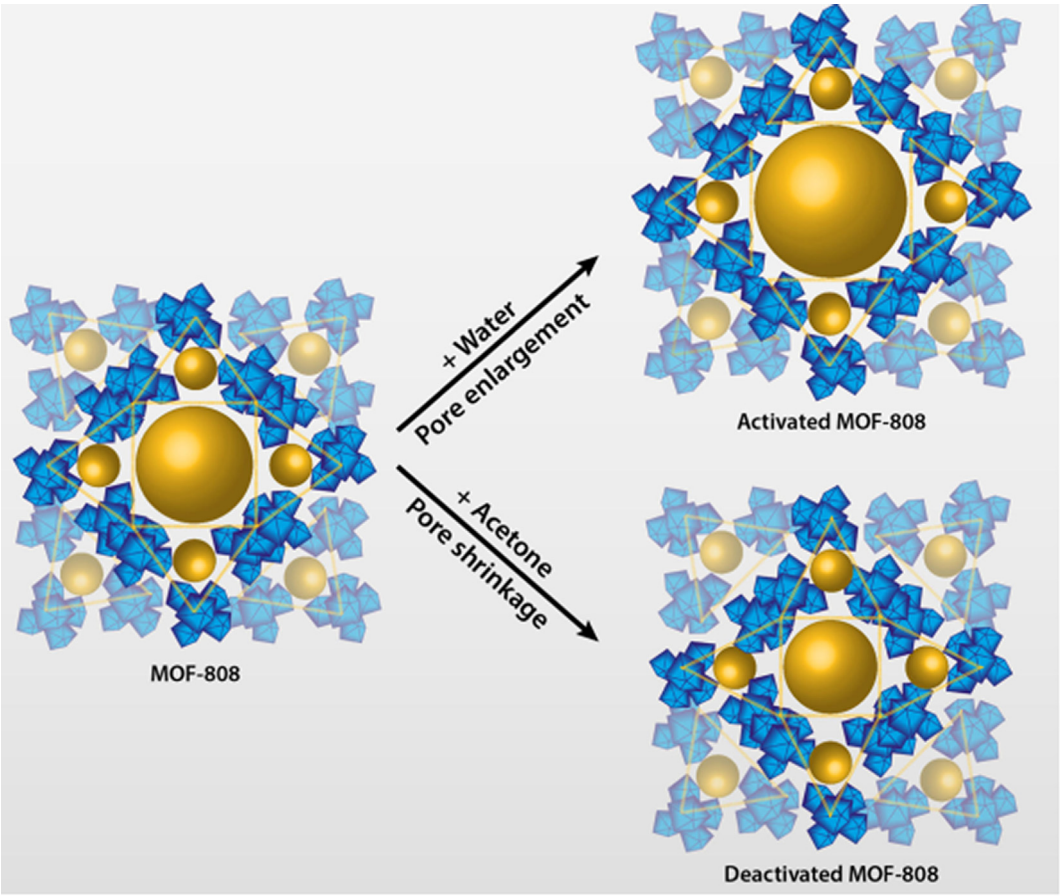

Fig. 7. Hydractivation of pore expansion route with water after vacuum drying and hydradeactivation of pore shrinkage route with acetone after vacuum drying [38].

by the pristine polyamide thin-film composite membrane was 8.3 L/m^2·h·bar, the polyamide/UiO-66 membrane showed significantly improved water permeance by approximately 85% (15.4 L/m^2·h·bar) by addition of 0.2 w/v% UiO-66 nanoparticles (pore size and functionalized analogs = 0.6–1.0 nm [98]) with a similar degree of solute rejection (50–99%). These findings were of interest as the thickness of the polyamide/UiO-66 membrane (230 nm) was larger than that of the pristine polyamide membrane (205 nm). In general, solvent permeance by membranes with comparable pore structures decreases with increasing membrane thickness [99]. However, the thicker MOF membrane showed significantly improved organic solvent permeance, particularly for isopropanol, presumably due to the basic porosity of MOFs,

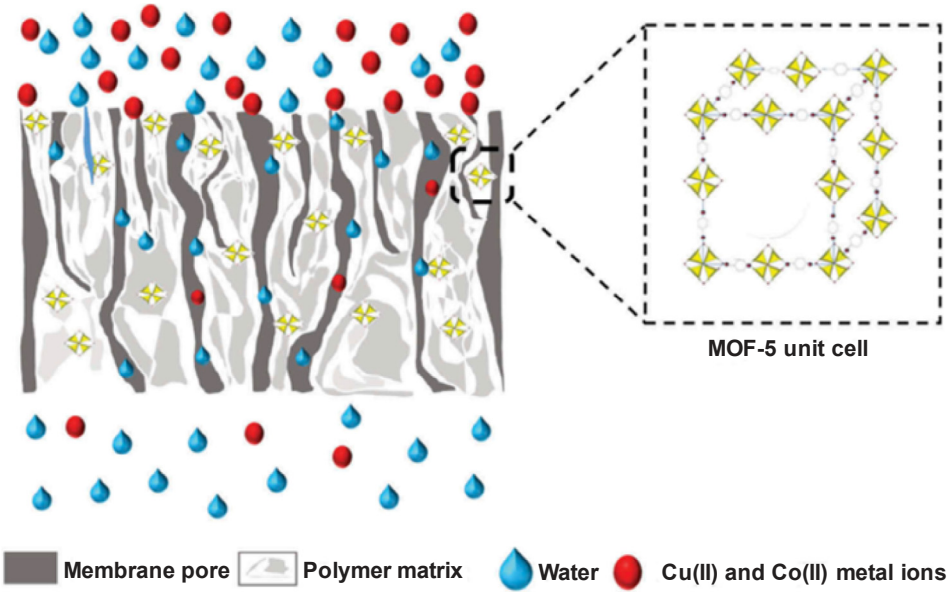

Fig. 8. Schematic representation of removal of heavy metal ions from aqueous solution by MOF-5-incorporated membrane nanofiltation [92].

which was also consistent with a previous study; the isopropanol permeance of polyamide/UiO-66 membranes was nearly double that of polyamide/cyclodextrin composite membranes [100]. The order of dye removal by the polyamide/UiO-66 membrane was rose Bengal > thiazole yellow G > crystal violet > safranin O > methyl orange, implying dependence on dye molecular weight.

Gnanasekaran et al. investigated the effects of MOF-5-embedded polymeric membrane properties on the removal of heavy metals based on porosity, pore size, hydrophobicity, water permeation, and antifouling behavior [92]. The average pore diameter of polyethersulfone and cellulose-acetate-based MOF-5 membranes increased from 11.2 to 13.9/7.8 to 8.6 nm, and the membrane porosity also increased from 70° to 78°/72° to 81% due to the presence of MOF-5 in the polyethersulfone/cellulose acetate casting solution, respectively. The hydrophobicity of the MOF-polymer membrane based on contact angle decreased with the addition of different polymers, i.e., polyethersulfone, cellulose acetate, and polyvinylidene fluoride, from 86° to 76°, 75° to 70°, and 80° to 73°, respectively, indicating that the hydrophobicity of MOF-polymer membranes is significantly lower than that of the pristine membrane [101–103]. The increase in pore size/porosity and decrease in hydrophobicity made significant contributions to the membrane permeability and resistance. The permeability increased from 29.5 to 53.3 and 41.0 to 69.7 L/m^2·h, while the hydraulic resistance decreased from 13 × 10^{13} to 7.4 × 10^{13} and 9.6 × 10^{13} to 5.6 × 10^{13} 1/m for polyethersulfone/MOF-5 and cellulose acetate/MOF-5, respectively. Overall, the MOF-polymer membranes showed significantly higher removal efficiency (56–58% for Cu^{2+} and 67–79% for Co^{2+}) than the pristine polymeric membrane (35–55% for Cu^{2+} and 44–61% for Co^{2+}) [92].

2.3.3. Flux and removal

Polyacrylonitrile/MOF-808 NF membranes have been used for the removal of Cd^{2+} and Zn^{2+} in the presence of co-ions [38]. The MOF membranes showed significantly enhanced maximum adsorption capacities of Cd^{2+} and Zn^{2+} (225 and 287 mg/g, respectively), while maintaining high water permeance (870 L/m^2·h·bar). The removal effectiveness of the selected heavy metal (Cd^{2+}) decreased by nearly 20% for all MOF membranes in the presence of co-ions, such as Na^+, Mg^{2+}, and Ca^{2+}, presumably due to competition for the adsorption sites of the MOF membranes between the heavy metals and the co-ions with different Pauling electronegativities (χ): 0.93, 1.31, 1.00, and 1.69 for Na^+, Mg^{2+}, Ca^{2+}, and Cd^{2+}, respectively [104]. In a separate study, TFN membranes incorporating UiO-66 were evaluated to determine removal of Se and As as well as NaCl, $MgCl_2$, Na_2SO_4, and $MgSO_4$ using a dead-end filtration unit at 10 bar [39]. The salt removal followed the order: $MgSO_4$ > Na_2SO_4 > $MgCl_2$ > NaCl. These findings may be explained by steric exclusion and electrostatic repulsion mechanisms: the relatively large hydrated SO_4^{2-} with a radius of 0.379 nm was rejected to a greater extent than was the smaller Cl^- (radius = 0.332 nm) [85]; divalent SO_4^{2-} was rejected to a greater extent by the more negatively charged MOF TFN membranes with −COOH functional groups than was monovalent Cl^- by the pristine thin-film composite membranes. The rejection of Se and As (82–97% for SeO_3^{2-} and 91–99% for $HAsO_4^{2-}$) was significantly improved by MOF membranes due to the holes of UiO-66 nanoparticles through which water molecules can readily pass, while the ions were selectively repelled. For Se species, higher removal of divalent anionic SeO_4^{2-} (Se(VI)) has been predicted compared to monovalent $HSeO_3^-$ (Se(IV)) at a solution pH of 7.5 [105].

The ZIF-8-based hollow nanocube TFN membrane exhibited significantly enhanced water permeance for Na_2SO_4 (19.4 L/m^2·h·bar) and NaCl (14.5 L/m^2·h·bar), nearly double those of the thin-film composite membrane [94]. These findings may be explained as follows: (i) The H_2O molecules readily move through the wet membrane surface/inner pores with hydrophilic nanocubes [106]; (ii) the inner hollow space of hydrophilic hollow nanocubes provides favorable flow channels and decreases the mass transfer resistance by reducing the diffusion space [107]; and (iii) the produced boundary region between hydrophilic hollow nanocubes and the polyamide polymer provides greater pathways for water passage [108]. For both humic acid and bovine serum albumin feed solutions, the ZIF-8-based hollow nanocube TFN membrane exhibited a much lower water permeance decline than the thin-film composite membrane, presumably due to the enhanced hydrophilicity and negative surface charge of the GO-TFN membrane [109]. Liu et al. reported that hydrophilic HKUST-1/reduced GO membranes exhibited excellent water flux, removal, and antifouling performance for methylene blue and Congo red [50]. While a conventional cellulose acetate membrane showed low removal of methylene blue and Congo red, HKUST-1/reduced GO membranes showed significantly improved removal of these dyes (89% and 80%, respectively). In addition, the HKUST-1/reduced GO membranes showed increased water flux of up to 33-fold (163 L/m^2·h) compared to the pristine membranes due to the increases in membrane interlayer space and channels [110].

The removal of two pharmaceuticals (diclofenac and naproxen, > 99%) was significantly enhanced by a polyamide/HKUST-1 bilayered TFN membrane, while an MOF membrane also showed increased membrane permeance from 6.8 L/m^2·h·bar to 33 L/m^2·h·bar [96]. The modified properties of the MOF membrane based on porosity, hydrophilicity, and surface roughness contributed to the improved performance. Yang et al. reported that ZIF-8@GO polyethyleneimine membranes showed higher water permeance (3.5 L/m^2·h·bar) compared to ZIF-8 polyethyleneimine membranes, while both membranes showed outstanding removal of methylene blue (> 99%) in methanol. The potential transport mechanisms for the membranes are outlined in Fig. 9. In particular, the permeance of the ZIF-8 polyethyleneimine membrane was enhanced due to the well-developed channels through which methanol molecules can readily pass.

2.4. UF membranes

2.4.1. Synthesis methods

While UF membranes are relatively practical in terms of operation,

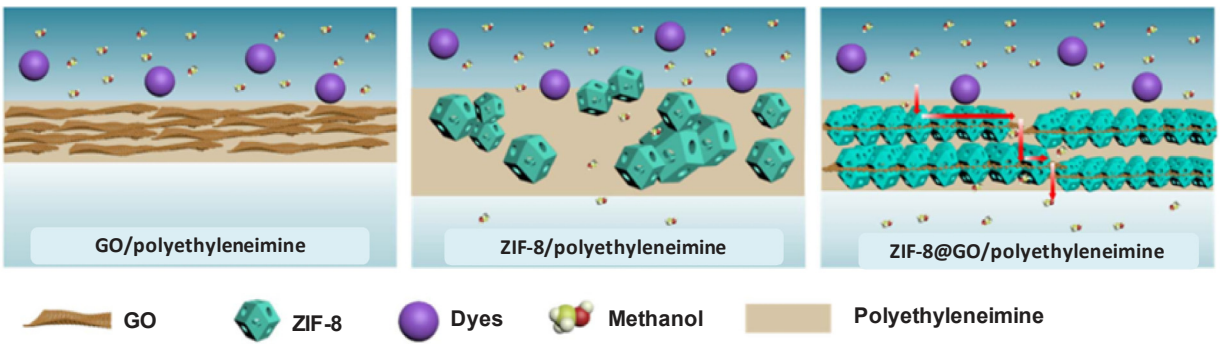

Fig. 9. The schematic of the dye molecules retention of GO/polyethyleneimine, ZIF-8/polyethyleneimine, and ZIF-8@GO/polyethyleneimine membranes [97].

cost, and maintenance compared to FO, RO, and NF processes, a key drawback in using a UF membrane is reduced performance due to membrane fouling [111]. Membrane modification with incorporation of MOFs is an attractive method to resolve this issue. Alumina hollow fiber membranes incorporating UiO-66 nanoparticles have been fabricated and reported to show outstanding humic acid removal and water flux [48]. To prepare the ceramic support, a sintering process following the phase inversion method was applied with various alumina powder sizes (1:2:7 ratio of 0.01:0.05:1 μm). UiO-66 nanoparticles were prepared using the solvothermal method [112]. Gholami et al. also employed the immersion precipitation phase inversion technique to fabricate hydrophilic polyethersulfone UF membranes with incorporation of TMU-5 MOF particles, which were tested with a milky oil–water feed solution [30]. ZIF-8 nanoparticles were immobilized on the trimesoyl chloride-polyvinylidene fluoride membrane surface functionalized with polyacrylic acid by in situ polymerization of $C_3H_3NO_2$ monomer and N,N′-methylenebisacrylamide cross-linker [113].

UiO-66 nanoparticles were attached to hydrophilic GO nanosheet layers as porous modifiers, which created unique nanocomposite properties by inhibiting stacking of the GO layers [42]. UiO-66@GO nanocomposites were employed to fabricate UiO-66@GO polyethersulfone membranes with high antifouling and water purification performance. Makhetha et al. used Cu terephthalate MOFs incorporating GOs to fabricate a series of polyethersulfone membranes through a phase inversion technique for dye removal [114]. A high flux biocatalytic MOF membrane was fabricated by 3D modification with polyethyleneimine, MOFs, and laccase/polydopamine [48]. Several water-stable MOFs, including MIL-101-L, MIL-101-S, UiO-67, UiO-66-NH_2, and UiO-66, were employed to modify the polyacrylonitrile support layer with incorporation of polyethyleneimine polymers. The biocatalytic membrane exhibited high water flux and a high degree of contaminant removal over a wide range of pH conditions and fair reusability. Fig. 10 presents a schematic diagram of the biocatalytic MOF membrane fabrication.

MIL-53(Fe)/polyvinylidene fluoride membranes were fabricated by a novel mixing technique in acetone and thermally induced phase separation that achieved homogeneous dispersion of very high percentages of MOF nanoparticles (10%, 33%, and 67%) in the membrane [44]. The MIL-53(Fe)/polyvinylidene fluoride membrane exhibited great performance for methylene blue retention and high water flux due to adsorption and catalytic oxidation. Sun et al. also employed a phase-inversion technique to fabricate superhydrophilic UiO-66-NH_2 MOF membranes functionalized with poly(sulfobetaine methacrylate) incorporated into a casting solution of polysulfone [115]. One of the key challenges during membrane fabrication using the phase-inversion method is to disperse raw MOF particles uniformly, particularly due to the poor dispersion of raw UiO-66-NH_2 particles in the polysulfone casting solution. The problem was resolved using poly(sulfobetaine methacrylate) brushes produced near the MOF particles that successfully inhibited the aggregation and improved the degree of dispersion.

2.4.2. Membrane properties

The comprehensive performance of Cu terephthalate@GO polyethersulfone membranes was evaluated based on dye removal and antifouling behavior [114]. Addition of Cu terephthalate and/or GO to the polyethersulfone support increased water flux compared to the pristine polyethersulfone membrane, as the hydrophilic properties of porous GO nanosheets decrease tortuosity by providing additional wide flow channels where H_2O molecules can readily travel through the MOF composite membrane [47]. The removal of dyes (methylene blue, Congo red, and methyl orange) varied depending on the properties of membranes and dyes. In general, the negatively charged MOF@GO membrane with acidic functional groups exhibited greater dye removal than the pristine polyethersulfone membrane. The MOF@GO membrane also showed higher flux recovery ratio (> 70%) at all MOF and/or GO loadings than the pristine polyethersulfone membrane (43%), indicating that the MOF membrane had better antifouling behavior increasing the lifespan of the membrane [110].

In another study, self-cleaning polyacrylonitrile-co-maleic acid-polyethyleneimine-Ag-modified polyethersulfone membranes were fabricated, and shown to have hydrophilic and antibacterial properties [116]. Excellent antibiofouling was observed by the self-cleaning MOF membrane containing antimicrobial Ag nanoparticles and negatively charged/hydrophilic amine functional groups. The antibiofouling mechanism of the self-cleaning MOF membrane is presented in Fig. 11. Microorganisms that come into contact with the membrane surface are inactivated by the antimicrobial Ag nanoparticles by rupturing their negatively charged plasma membrane, which causes the release of negatively charged proteins, while the highly hydrophilic/negatively charged −OH and $-NH_2$ functional groups inhibit the accumulation of these proteins on the membrane surface due to electrostatic repulsion [116].

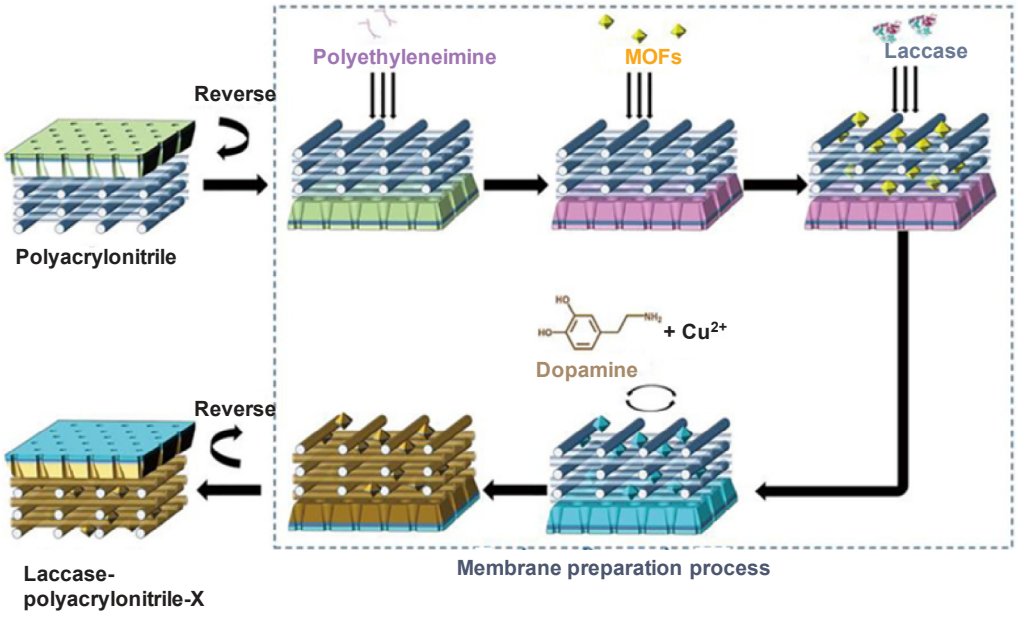

Fig. 10. Schematic diagram of biocatalytic membrane preparation [43].

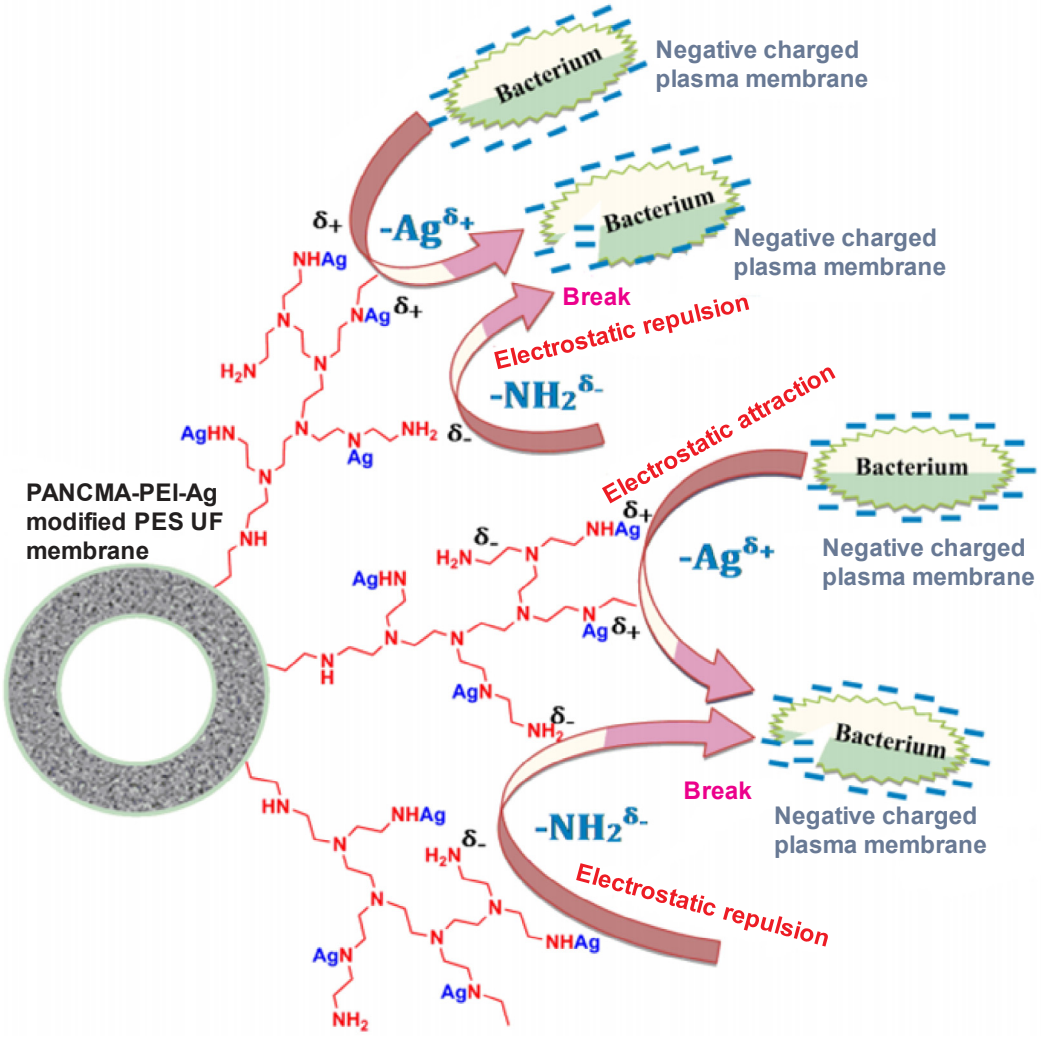

Fig. 11. Schematic representation of the self-cleaning property of the membrane [116].

Mechanical strength is one of the main requirements for the practical application of UF membranes [117]. Sun et al. investigated the mechanical strength of hydrophilic hollow ZIF-8/polysulfone membranes prepared by the surface functionalization-based etching method combined with tannic acid [118]. Addition of ZIF-8 particles rapidly reduced elongation of the polysulfone membrane (approximately 15–8%) with comparable elasticity, which was somewhat consistent with the results of a previous study in which the incorporation of different constituents into polysulfone membranes reduced the UF membrane strength [119]. However, the elasticity and elongation of the hollow ZIF-8/polysulfone membrane placed into tannic acid solution (3000 mg/L) increased by approximately 20% (1.5 MPa), indicating that the ZIF-8 nanoparticles with tannic acid improved the mechanical strength of the membranes. The improvement was likely due to the uniform distribution of ZIF-8 nanoparticles in the polysulfone membrane and the strong formation of H-bonds between the −OH groups on the nanoparticle surface and -SOO groups on the polyethersulfone chain [120].

2.4.3. Flux and removal

A UiO-66/alumina hollow-fiber membrane was tested to evaluate the removal of humic acid and membrane water flux [48]. The MOF membrane pure water flux decreased to 41.1 L/m^2·h, which was much lower than the pristine alumina hollow-fiber membrane (231 L/m^2·h), and this was presumably due to the presence of UiO-66 nanoparticles coating the whole surface of the membrane. However, during filtration with 1000 mg/L humic acid, the pristine membrane showed a significant reduction of water flux (41.1 L/m^2·h) due to humic acid fouling on the membrane surface and/or pores [121]. The water flux of the MOF membrane under the same conditions decreased slightly to 25.7 L/m^2·h due to electrostatic repulsion between the MOF particles and humic acid molecules, which was still significantly higher than that of the pristine membrane, while these membranes showed similar humic removal (93–98%). In another study, a polyethersulfone TMU-5 membrane was evaluated for membrane fouling during oil–water separation filtration with a milky oil–water feed solution (up to 40,000 mg/L) in a dead-end cell unit [30]. The flux of the pristine polyethersulfone membrane decreased significantly in the presence of a high concentration of milk powder. After cleaning of the membrane, the pure water flux of the pristine membrane (contact angle = 67° and surface roughness = 44 nm) showed poor recovery (flux recovery ratio = 25%), while a much higher flux recovery ratio was obtained with the MOF membrane (98%) due to the membrane hydrophilicity and surface roughness change (contact angle = 53° and surface roughness = 5.2 nm).

Synthetic wastewater containing Ni(II) (2 mg/L) and Na^+ (15,000 mg/L) at pH 5.5 was effectively treated by polyacrylic acid/ZIF-8/polyvinylidene fluoride membranes [113]. During a four-cycle filtration period with an effective treatment volume in each cycle (1870, 1307, 958, and 453 L/m^2), Ni(II) was removed effectively at the beginning of each cycle (0.1 mg/L) and increased somewhat with increasing treatment volume. The findings with the maximum adsorption

capacity of 220 mg-Ni(II)/g imply that the removal of Ni(II) is due mainly to adsorption on the MOF membrane associated with electrostatic attraction and hydrogen bonding, particularly among Ni(II), −OH groups on MOFs, and −COOH groups in the polyacrylic acid layer. Ma et al. compared the performance of three different membranes (polyethersulfone, GO/polyethersulfone, and UiO-66@GO polyethersulfone) in terms of membrane fouling, water flux, and dye removal using methyl orange and Direct Red 80 [42]. While the pristine polyethersulfone membrane showed fair removal of these dyes, the GO/polyethersulfone and UiO-66@GO polyethersulfone membranes showed greater removal (93% and 94% for methyl orange; 85% and 87% for Direct Red 80, respectively). The UiO-66@GO polyethersulfone exhibited much higher water flux than the polyethersulfone and GO/polyethersulfone membranes (approximately 350% and 80%, respectively). In addition, the UiO-66@GO polyethersulfone membrane (89%) had a higher flux recovery ratio compared to the polyethersulfone and GO/polyethersulfone membranes (43% and 84%, respectively).

During methylene blue removal, the MIL-53(Fe)/polyvinylidene fluoride membrane showed nine-fold enhancement in effective treatment volume with a water flux of approximately 225 L/m^2·h, while dye removal was maintained at > 75% [44]. The reasons for the excellent performance of the MOF membrane are as follows: (i) The increase in hydrophilicity of the membrane with ultrahigh MOF loading (67%) allows ready transport of water molecules through the membrane [122]; (ii) during the process of MOF membrane fabrication, numerous pores are produced that provide water transport channels, while the pristine polyvinylidene fluoride membrane showed no observable pores in cross-sectional images [42]; and (iii) the MOF membrane had a very rough top surface compared to the pristine membrane, increasing the effective filtration area and thus improving the membrane water flux [115]. In addition, free hydroxyl radicals produced in the presence of H_2O_2 and Fe(III) in dye solution enhance the degradation of methylene blue, while the dye is removed mainly due to adsorption on the MOFs incorporated in the membrane [44]. The mechanisms of multifunctional concurrent dye removal by the MOF membrane are described in Fig. 12. Table 1 summarizes the performance of FO, RO, NF, and UF membranes incorporating various MOFs and key findings.

3. Conclusions and areas of future study

Since the introduction of MOFs to environmental applications, a great deal of progress has been made in using MOFs, particularly in FO, RO, NF, and UF membrane processes for water purification. Various preparation methods, such as TFN, (porous) mixed matrix, the solvothermal method, the electrodeposition method, and vacuum filtration have been employed to fabricate MOF-based membranes to improve membrane performance, particularly in terms of water flux and membrane fouling. Numerous studies have shown significantly enhanced water flux, antifouling, and solute selectivity by MOF-based membranes incorporating various MOFs (e.g., copper 1,4-benzenedicarboxylate, MIL-53, Cu-BTC, MIL-100, UiO-66, ZIF-8, MIL-125, HKUST-1, Zn-based MOF-808, MIL-101(Cr), and MIL-101(Fe)) on various ultrathin films containing active/support layers (*e.g.*, polyamide, polydopamine, polyimide, polysulfone, polyacrylonitrile, polyethersulfone, cellulose acetate, and polyvinylidene fluoride). In particular, the performance of MOF-based FO/RO/NF/UF membranes has been shown to be significantly improved by modifying the membrane properties: (i) MOF-based membranes have high tunable porosities, extra channels, and accessible large surface areas, which improve water transport through the membranes; and (ii) these hydrophilic MOFs have a high capacity to combine particular species/functionalities easily without changing the framework topology, which is advantageous to reduce membrane fouling and enhance membrane selectivity due to steric exclusion and electrostatic repulsion. In addition, the employment of MOFs into FO/RO/NF/UF membranes could importantly enhance the roughness and durability of membranes, thus extending large-scale industrial application.

However, these MOF-based membrane studies were limited to a few MOFs, a few solutes (NaCl, dyes, and heavy metals), and laboratory-scale short-term tests under restricted water chemistry and operating conditions. Therefore, a comprehensive performance evaluation of various MOF-based membranes for different contaminants in varying water-quality and operation environments is essential particularly: to investigate the effects of different MOFs on membrane fabrication and properties in terms of hydrophilicity, pore size, and surface roughness, as it is challenging to determine the interactions between casting compounds or MOFs, the uniformity of MOF dispersion in different solvents, development of efficient incorporating techniques, and post-treatment techniques to reduce deficiencies of PMMs; to effectively compare a “trade-off” in terms of water permeance and salt removal among MOF-based FO, RO, NF, and UF membranes; to examine the transport mechanisms of different MOF-based membranes in the presence of various background ions and natural organic matter to simulate natural waters; and to assess larger-scale membrane stability/long-term processes combined with membrane bioreactors as there are inadequate pilot/full-scale data regarding MOF-based FO, RO, NF, and UF membranes for large-scale applications.

The chemical stability of MOF embedded within each category of membrane and the hydrolytic stability of MOF-based membranes is vital to the evaluation of these MOF-based membranes for real application of water purification. In particular, the select of solution pH during membrane filtration might result in simple degradation of certain MOF structures, occasionally to the point of thorough damage or change of the original phase and resulting in loss of most if not all

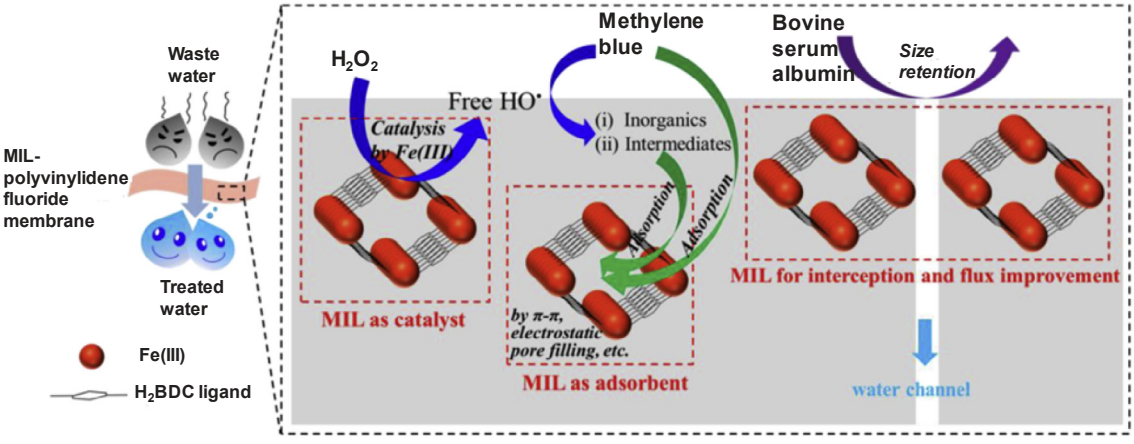

Fig. 12. Mechanism of multifunctional simultaneous decontamination by MIL-polyvinylidene fluoride membranes [44].

Table 1
Summary of MOF-based membranes for FO, RO, NF, & UF and their performance.

Membrane class	MOF based membrane	Experimental condition	Key performance	Key finding	Ref.
FO	MOF- thin-film based PMM	Caspian seawater and orange juice DS = NaCl 0.5 and 2 M	Flux = 141 L/m^2-h B/A = 55 kPa Salt rejection = 90.1%	Thin-film based porous matrix membranes could significantly enhance water permenance in FO processes owing to suitable porosity of porous segment, thin thickness, and small tortuosity by the rejection of MOF particles.	[32]
	Porous MOF (copper 1,4-benzenedicarboxylate nanosheet)/TFN	Wastewater effluent CFV = 15 cm/s	Flux = ~28 L/m^2-h B/A = 10 kPa	The MOF membrane for urban wastewater treatment discovered a greater water permeance and a clear antifouling tendency against the pristine one, owing to the reduced hydrophobicity and biocidal action of the membranes.	[59]
	GO-Ag-MOF TFN	Synthetic wastewater CFV = 8.5 cm/s	Biocidal activity = 96%	FO tests with feed-containing *E. coli* and sodium alginate pointed to determining anti-biofouling and antifouling behaviors of the GO − Ag-MOF membrane.	[70]
	MOF-based PMM	MOFs = MIL-53, Cu-BTC, and MIL-100 DS = $MgCl_2$ 0.1–3 M	Flux = PMM_{C300} > PMM_{A200} > PMM_{F300}	MOF-based porous matrix strategy could enhance not only the membrane bulk porosity but also decrease the membrane tortuosity.	[47]
	UiO-66 TFN	Synthetic water CFV = 0.95 cm/s DS = Na_2SO_4 0.25–1.25 M	Phenol red (> 99%), Na_2SO_4 (94–96%), NaCl (27%)	The self-standing thin films with enhanced microporosity exhibit high-performance FO membranes based on high water permeance, enhanced ion removal, and decreased internal concentration polarization.	[33]
	UiO-66/GO membrane	Synthetic wastewater CF rate = 5.6 L/h DS = NaCl 1, 2, and 4 M	Biocidal activity = 90% Flux = 29.2 L/m^2-h	When the incorporating ratio of UiO-66/GO is < 1:1, the doped UiO-66 didn't affect the layered structure of the membrane, and a smooth surface morphology is obtained.	[75]
	Polydopamine modified zeolitic imidazolate framework	Synthetic water CFV = 8.5 cm/s DS = $MgCl_2$ 1.0 M	Flux = 20.8 L/m^2-h Metal rejection = > 96% (Cu, Ni, & Pb) B/A = 3.6 kPa	The MOF nanoparticles give the selective layer with decent wettability and loose structure, by enhancing the affinity between the nanofillers and polyamide matrix, thus retaining the selectivity of membrane.	[76]
	Nanocomposite thin films incorporated with blue lemon polyoxometalate based open-framework	Synthetic wastewater CF rate = 200 mL/min DS = NaCl 1.0 M	Flux = 28.6 L/m^2-h NaCl rejection = 95.1%	The improved anti-fouling behaviors of changed membranes result from decrease in roughness and enhancement in membrane surface hydrophilicity.	[123]
	Silver-based MOFs to surface functionalization of TFN	Synthetic wastewater DS = NaCl 0.5–2.0 M	Flux = 0.94 L/m^2-h-bar Biocidal activity = > 99%	The functionalization process developed a constant distribution of Ag-MOFs on the active locations of polyamide layer rendering the membrane surface highly antibacterial and anti-biofouling behavior.	[124]
	MOF-cellulose acetate triacetate membrane	Synthetic seawater CFV = 21 cm/s DS = NaCl 0.5–2.0 M	Flux = ~30 L/m^2-h NaCl rejection = 95.1%	Hydrophilic surface and highly porous structure of Cu-benzene-1,3,5-tricarboxylate nanoparticles could selectively absorb water and give different passage pathways for water molecules through the membrane.	[34]
	MOF nanocrystals-PES membrane	Synthetic seawater CFV = 21 cm/s DS = NaCl 0.5–2.0 M	Flux = ~35 L/m^2-h Flux decline = 7%	The MOF nanocrystals developed a more hydrophilic surface of the modified membranes, and provided a lesser transport resistance in their selective layer.	[125]
RO	Polyamide thin-film-nanocomposite/ zoitic midazolate framework-8	Synthetic water Cross-flow NaCl = 2,000 mg/L Pressure = 15.5 bar	Permeance = 3.35 L/m^2-h-bar NaCl rejection = 99%	Hydrophobic microporous fillers ZIF-8 provided higher water permeance increase ratio than the hydrophilic fillers having zeolite 4A.	[78]
	Zeolitic imidazolate framework-8	Water desalination Molecular simulation	Activation energy = 24.4 kJ/mol	Water molecules in ZIF-8 membrane are less hydrogen-bonded and the period of hydrogen-bonding is considerably longer.	[83]
	TFN membrane filled with UiO-66 and MIL-125	Synthetic water Cross-flow NaCl = 2,000 mg/L Pressure = 300 psi	Flux = 74.9 (UiO-66) and 85.0 (MIL-125) L/m^2-h NaCl = > 98.5%	The high permeance results indicate filling of MOFs in TFN membrane could be helpful owing to the nanoparticles having an organic part.	[35]
	TFN membrane based metal organic complexes	Brackish water Cross-flow NaCl = 7,000 mg/L Pressure = 5 bar	Flux = 41 L/m^2-h NaCl rejection = 97%	These MOFs were incorporated with the polyamide layer of thin film composite membrane to improve the water permeance with more solute selectivity.	[126]

(*continued on next page*)

Table 1 (*continued*)

Membrane class	MOF based membrane	Experimental condition	Key performance	Key finding	Ref.
	Polysulfone membrane containing MOF (HKUST-1)	Synthetic water Cross-flow NaCl = 2,000 mg/L Pressure = 250 psi	Flux = 47 L/m^2-h NaCl rejection = 97%	Both the membrane hydrophilicity and porosity were enhanced in the acid-MOF membrane, owing to the addition of hydrophilic functional groups and the solid bonding between the Cu ions and the cluster.	[79]
	P$^+$GO-anchored copper- and trimesic-acid-based MOF membrane	Synthetic water Dead-end NaCl = 250–2,000 mg/L Pressure = 0.69 MPa	Flux = ~20 L/m^2-h Bovine serum albumin = 98.8% NaCl = 96.8–99.9%	These membranes were capable enough to exhibit continuous permeation of water even after 15 d constant run and had a flux value of 16.97 L/m^2-h.	[80]
	Polyamide@NH2_MIL-88B nanocomposite	Synthetic water Cross-flow Phenol = 100 mg/L Pressure = 15 bar	Flux = 23.5 L/m^2-h Phenol rejection = 92%	The NH_2_MIL-88B interlayer embedded in the polyamide coating improved the transport pathways and decreased the cross-linking degree and membrane thickness,	[37]
	TFN membranes doped with MIL-101(Cr) nanoparticles	Synthetic water Cross-flow NaCl = 2,000 mg/L Pressure = 16 bar	Permeance = 2.2 L/m^2-h-bar NaCl = > 99%	The porous configurations of MIL-101(Cr) could create direct water channels in the dense selective polyamide layer for water molecules to pass through quickly, causing the increasing water flux of membranes.	[36]
NF	Polyamide/hydrostable MOFs	Synthetic water Dead-end Co = 200–1,000 mg/L Pressure = 5 bar	Permeance = 15.4 L/m^2-h-bar Rose bengal = > 99% Azithromycin = > 97.6%	The water fluxes of PA/UiO-66 composite membranes were 200% higher than those of pristine polyamide membranes during long-term continuous operation, suggesting excellent anticompaction performances.	[91]
	Zr-based MOF-808 nanofibrous membrane	Synthetic water Dead-end/adsorption Cd(II)/Zn(II) = 20 mg/L Pressure = 0.4 bar	Flux = 348 L/m^2-h q_m = 225 for Cd and 287 for Zn (mg/g)	The polyacrylonitrile/MOF-808 “hydractivated” composite membrane treated about 600 mL of Cd, while the traditional vacuum-activated composite treated 460 mL.	[38]
	Zn-based MOF embedded polymeric membranes	Synthetic wastewater Dead-end Cu(II)/Co(II) = 1,000 mg/L Pressure = 10 bar	Flux = 69.7 L/m^2-h Co(II) rej. = ~75% Cu(II) rej. = ~55%	The hydrophilic properties and performance of composite membranes are enhanced by the incorporation of MOF-5 due to the metal clusters of MOF-5	[92]
	UiO-66 incorporated TFN membranes	Synthetic water Dead-end Se/As = 1,000 mg/L Pressure = 10 bar	Permeance = 11.5 L/m^2-h-bar $SeO_3^{2-}/SeO_4^{2-}/HAsO_4^{2-}$ = 96.5/97.4/98.6%	The improved performance of TFN membranes compared to relatively traditional NF membranes was due to the improved hydrophilicity, exceptional aperture and highly porous structure of UiO-66.	[39]
	Interfacial synthesis of ZIF-8 membranes	Synthetic water Dead-end Rose Bengal = 17.5 μM Pressure = 2 bar	Permeance = 90 L/m^2-h-bar Rose Bengal = 85%	Higher molar ratios of 2-methlyimidazole to zinc nitrate cause denser membranes with smaller permeance and greater removal, owing to the dense packing and smaller inter-particle spaces.	[127]
	Hydrophilic hollow nanocube derived from ZIF-8/functionalized TFN membrane	Synthetic water Cross-flow Na_2SO_4 = 1,000 mg/L Pressure = 8 bar	Permeance = 19.4 L/m^2-h-bar Na_2SO_4 $^-$ = 95.2% FRR = 93.2%	The flux recovery ratios of the MOF membrane are 93 and 85% corresponding to humic acid and bovine serum albumin solutions, respectively.	[94]
	Polydopamine-modified reduced RO/MOFs nanocomposite	Synthetic water Vacuum suction Methylene blue = 40 mg/L Pressure = 0.09 MPa	Flux = 185 L/m^2-h Methylene blue = 99.8% FRR = 82.9%	HKUST-1 inserted into GO nanosheets improved inter-layer spacing, and polydopamine played an important role in decrease and combination, which improved membrane separation effectiveness and flux.	[50]
	Ce-MOF/polyethersulfone mixed matrix membrane	Synthetic water Dead-end Dye = 30 mg/L Pressure = 3 bar	Flux = 21.2 L/m^2-h Dye removal = 99% FRR = 99.4%	The antifouling behavior of the modified membranes was enhanced and the sensibility of the membranes to fouling decreases with a reduction in the roughness of their surfaces.	[128]
	TFN membrane with the minimum amount of MOF (MIL-101(Cr))	Synthetic water Dye in methanol Dead-end Dye = 20 mg/L Pressure = 20 bar	Methanol permeance = 10.1 L/m^2-h-bar Rose Bengal = > 90%	Defect-free MOF membranes containing a monolayer have been obtained with an exceptional nanofiltation performance of methanol/dye solutions due to the large MIL-101(Cr) pore system.	[40] [96]

(*continued on next page*)

Table 1 (*continued*)

Membrane class	MOF based membrane	Experimental condition	Key performance	Key finding	Ref.
	Polyamide/MOF bilayered TFN membranes	Diclofenac/naproxen Dead-end Co = 1 mg/L Pressure = 20 bar	Permeance = 33.1/24.9 L/m^2-h-bar Removal = > 98%	The MOF membranes improved their performance due to the MOF porosity, membrane hydrophilicity, polyamide layer thickness, and membrane roughness.	
	Amino-Functionalized MOF/GO composite membrane	Synthetic water Cross-flow Cu(II) = 200 mg/L Pressure = 0.7 MPa	Flux = 31 L/m^2-h Rejection = ~ 90% q_m = 254 (mg/g) at pH 5.0	Innovative and highly efficient NF membrane could be simply fabricated through surface decoration of IRMOF-3/GO onto polydopamine-coated polysulfone substrate.	[93]
	MIL-53(Al) nanocomposite membrane	Cross-flow Nitroso-R salt/xylenol orange/ponceau S Co = 500 mg/L Pressure = 1.0 MPa	Flux = 40.6 L/m^2-h Nitroso-R salt/xylenol orange/ponceau S = 83.9/98.3/99.8%	Once the molecular weight is 670 Da, the polyethylene glycol removal is < 35%. However, the removal of xylenol orange (molecular weight 673 Da) is almost 99%, which is caused by the size exclusion and electrostatic repulsion.	[41]
UF	UiO-66 Alumina hollow fiber Solvothermal	Cross-flow Humic acid Co = 1, 000 mg/L ΔP = 2 bar	Flux = 68 L/m^2-h Removal = 99%	Ceramic membranes incoroporated with UiO-66 particles could be beneficial for humic acid removal. The optimum condition for using this membrane appeared to be at pH ≥ 9.	[48]
	TMU-5 PES membrane bending/sonication	Dead-end Oil-water Co = 40,000 mg/L ΔP = 3 bar	Flux = 123 kg/m^2-h Removal = > 98% FRR = 25.5–98.7%	Membranes having hydrophilic surfaces are less delicate to fouling than hydrophobic membranes, and the efficiency to recover the performance.	[30]
	Porous matrix membrane using hydrophilic MOFs (MIL-53, Cu-BTC, and MIL-100)	Cross-flow Humic acid Co = 1, 000 mg/L ΔP = 5 bar	Flux = ~175–250 L/m^2-h Removal = > 90 (dextran)	Porous matrix membrane could noticeably enhance water permeance possibly due to the removal of MOF particles in the polymer matrix, which enhanced membrane porosity and interconnectivity of the membrane.	[57]
	Polyacrylic acid/ZIF-8/polyvinylidene fluoride	Synthetic water Adsorption Ni(II) removal	q_m = 219–283 (mg/g) at various salinity conditions (Na = 0–15,000 mg/L)	The adsorption mechanism was apparently due to the electrostatic attraction by carboxyl groups in polyacrylic acid as well as particular H-bonding interaction between Ni(II) and hydroxyl on ZIF-8 frameworks.	[113]
	UiO-66@GO/polyethersulfone Solvothermal	Dead-end Direct Red 80 Co = 200 mg/L ΔP = 2.5 MPa	Flux = ~15 kg/m^2-h Removal = 98.3% FRR = 88.6%	The water permeance of composite membrane with UiO-66@GO loading exhibits an increase of 35% and 78% respectively in comparison with that of the polyethersulfone and GO/polyethersulfone membranes.	[42]
	Cu(terephthalate)@ GO/polyethersulfone	Dead-end Methylene blue Congo red Methyl orange Co = 100 mg/L ΔP = 200 KPa	Flux = ~150 L/m^2-h Removal = ~20–90% FRR = ~90%	Alternate pure water flux pathways through the matrix were created through the porous MOFs causing decreased tortuosity and thus enhanced permeate flux in Cu (terephthalate)@GO/polyethersulfone composite membranes compared with pure polyethersulfone membrane.	[114]
	MIL-101(Cr)-laccase-polyacrylonitrile	Dead-end Bisphenol A Co = 10 mg/L ΔP = 1 bar	Flux = 708 L/m^2-h Removal = 92%	The polymers in the selective separation layer can immobilize laccase mostly by electrostatic attraction, but did not change the morphology of membrane surface and permeability.	[43]
	67-MIL- polyvinylidene fluoride	Dead-end Methylene blue Co = 20 mg/L ΔP = 2 bar	Flux = ~250 L/m^2-h Removal = 60- > 95%	The 67-MIL-polyvinylidene fluoride membrane was accessible for long-term run and multiple contaminants removal in wastewaters.	[44]
	UiO-66- poly(sulfobetaine methacrylate)/ polysulfone	Cross-flow Bovine serum albumin Co = 500 mg/L ΔP = 0.2 MPa	Flux = ~600 L/m^2-h Removal = 98.5%	The obtained hybrid membrane exhibits highly improved water permeance and antifouling performance without losing much protein retention.	[115]
	Hollow zeolitic imidazolate framework-8	Cross-flow Synthetic water Bovine serum albumin	Flux = 597 L/m^2-h Removal = > 98%	The incorporation of hollow zeolitic imidazolate framework-8 rendered the membrane with improved resistance to fouling,	[118]

(*continued on next page*)

Table 1 (*continued*)

Membrane class	MOF based membrane	Experimental condition	Key performance	Key finding	Ref.
		Co = 500 mg/L ΔP = 0.2 MPa		suggesting the great application potential of such MOF/polymer hybrid UF membranes in wastewater treatment.	
	HKUST-1@GO	Dead-end	Flux = 184 L/m^2-h	The fabricated HKUST-1@GO hybrid membranes have more/larger pore channels and smoother membrane surface, owing to the structure of HKUST-1 and plentiful hydrophilic groups of GO.	[129]
		Bovine serum albumin Co = 1,000 mg/L ΔP = 0.15 MPa	Removal = > 98% FRR = 88%		
	Amino-functionalized MOF-ceramic membrane	Tubular filtration Pb(II) Co = 30 mg/L ΔP = 0.05 MPa	Flux = 400 L/m^2-h Removal = ~45% q_m = 1,795 (mg/g)	The adsorption mechanisms were noticed as coordination interaction between amidogen (–NH_2) and Pb(II).	[130]

CFV = cross flow velocity; B/A = solute permeability/water permeability, DS = draw solution; TFN = thin-film nanocomposite; FRR = water flux recovery ratio, q_m = adsorption capacity.

filtration capacity. This needs to be considered management and not certainty since there are other issues that may prohibit these processes to take place. In addition, since the currently high price of MOFs could prohibit the large-scale application of MOF-based membranes, new fabrication methods of MOFs are required, which focus on practical approaches associated with inexpensive and common raw materials. While this review mainly focuses on the performances of membranes in water purification, the systematic understanding of transport mechanisms of vital aqueous species by various MOF-based membrane is still necessary in terms of the porosity of membrane, the host–guest interactions, or macroscopic fluidic dynamic as well.

Declaration of Competing Interest

The authors declare that they have no known competing financial interests or personal relationships that could have appeared to influence the work reported in this paper.

Acknowledgements

This research was supported by the National Science Foundation, USA (OIA-1632824) and by the Korea Environment Industry & Technology Institute (KEITI) through Plant Research Program, funded by Korea Ministry of Environment (MOE) (88097). The present research has been conducted by the Research Grant of Kwangwoon University in 2018.

Appendix A. Supplementary material

Supplementary data to this article can be found online at https://doi.org/10.1016/j.seppur.2020.116947.

References

[1] D. Gollin, R. Jedwab, D. Vollrath, Urbanization with and without industrialization, J. Econ. Growth 21 (2016) 35–70.
[2] L. Dong, M. Dai, H.W. Liang, N. Zhang, N. Mancheri, J.Z. Ren, Y. Dou, M.M. Hu, Material flows and resource productivity in China, South Korea and Japan from, to 2008: A transitional perspective, J. Clean. Prod. 141 (2017) (1970) 1164–1177.
[3] P.S. Goh, A.F. Ismail, A review on inorganic membranes for desalination and wastewater treatment, Desalination 434 (2018) 60–80.
[4] A. Bhatnagar, M. Sillanpaa, A. Witek-Krowiak, Agricultural waste peels as versatile biomass for water purification – A review, Chem. Eng. J. 270 (2015) 244–271.
[5] S.A. Snyder, S. Adham, A.M. Redding, F.S. Cannon, J. DeCarolis, J. Oppenheimer, E.C. Wert, Y. Yoon, Role of membranes and activated carbon in the removal of endocrine disruptors and pharmaceuticals, Desalination 202 (2007) 156–181.
[6] S.A. Snyder, P. Westerhoff, Y. Yoon, D.L. Sedlak, Pharmaceuticals, personal care products, and endocrine disruptors in water: Implications for the water industry, Environ. Eng. Sci. 20 (2003) 449–469.
[7] Y. Yoon, J. Ryu, J. Oh, B.G. Choi, S.A. Snyder, Occurrence of endocrine disrupting compounds, pharmaceuticals, and personal care products in the Han River (Seoul, South Korea), Sci. Total Environ. 408 (2010) 636–643.
[8] L. Joseph, L.K. Boateng, J.R.V. Flora, Y.G. Park, A. Son, M. Badawy, Y. Yoon, Removal of bisphenol A and 17 alpha-ethinyl estradiol by combined coagulation and adsorption using carbon nanomaterials and powdered activated carbon, Sep. Purif. Technol. 107 (2013) 37–47.
[9] P. Westerhoff, Y. Yoon, S. Snyder, E. Wert, Fate of endocrine-disruptor, pharmaceutical, and personal care product chemicals during simulated drinking water treatment processes, Environ. Sci. Technol. 39 (2005) 6649–6663.
[10] L. Joseph, J. Heo, Y.G. Park, J.R.V. Flora, Y. Yoon, Adsorption of bisphenol A and 17 alpha-ethinyl estradiol on single walled carbon nanotubes from seawater and brackish water, Desalination 281 (2011) 68–74.
[11] C. Jung, L.K. Boateng, J.R.V. Flora, J. Oh, M.C. Braswell, A. Son, Y. Yoon, Competitive adsorption of selected non-steroidal anti-inflammatory drugs on activated biochars: Experimental and molecular modeling study, Chem. Eng. J. 264 (2015) 1–9.
[12] J. Heo, L. Joseph, Y. Yoon, Y.G. Park, N. Her, J. Sohn, S.H. Yoon, Removal of micropollutants and NOM in carbon nanotube-UF membrane system from seawater, Water Sci. Technol. 63 (2011) 2737–2744.
[13] S. Kim, K.H. Chu, Y.A.J. Al-Hamadani, C.M. Park, M. Jang, D.H. Kim, M. Yu, J. Heo, Y. Yoon, Removal of contaminants of emerging concern by membranes in water and wastewater: A review, Chem. Eng. J. 335 (2018) 896–914.
[14] Y.A.J. Al-Hamadani, K.H. Chu, J.R.V. Flora, D.H. Kim, M. Jang, J. Sohn, W. Joo, Y. Yoon, Sonocatalytical degradation enhancement for ibuprofen and sulfamethoxazole in the presence of glass beads and single-walled carbon nanotubes,

Ultrason. Sonochem. 32 (2016) 440–448.
[15] J.K. Im, J. Yoon, N. Her, J. Han, K.D. Zoh, Y. Yoon, Sonocatalytic-TiO2 nanotube, Fenton, and CCl4 reactions for enhanced oxidation, and their applications to acetaminophen and naproxen degradation, Sep. Purif. Technol. 141 (2015) 1–9.
[16] W.L. Ang, A.W. Mohammad, N. Hilal, C.P. Leo, A review on the applicability of integrated/hybrid membrane processes in water treatment and desalination plants, Desalination 363 (2015) 2–18.
[17] J. Farahbakhsh, M. Delnavaz, V. Vatanpour, Simulation and characterization of novel reverse osmosis membrane prepared by blending polypyrrole coated multiwalled carbon nanotubes for brackish water desalination and antifouling properties using artificial neural networks, J. Memb. Sci. 581 (2019) 123–138.
[18] K.H. Chu, M. Fathizadeh, M. Yu, J.R.V. Flora, A. Jang, M. Jang, C.M. Park, S.S. Yoo, N. Her, Y. Yoon, Evaluation of removal mechanisms in a graphene oxide-coated ceramic ultrafiltration membrane for retention of natural organic matter, pharmaceuticals, and inorganic salts, ACS Appl. Mater. Interfaces 9 (2017) 40369–40377.
[19] K.H. Chu, Y. Huang, M. Yu, J. Heo, J.R.V. Flora, A. Jang, M. Jang, C. Jung, C.M. Park, D.H. Kim, Y. Yoon, Evaluation of graphene oxide-coated ultrafiltration membranes for humic acid removal at different pH and conductivity conditions, Sep. Purif. Technol. 181 (2017) 139–147.
[20] L. Ding, Y.Y. Wei, Y.J. Wang, H.B. Chen, J. Caro, H.H. Wang, A two-dimensional lamellar membrane: MXene nanosheet stacks, Angew. Chem. Int. Edit. 56 (2017) 1825–1829.
[21] R.L. Han, X.F. Ma, Y.L. Xie, D. Teng, S.H. Zhang, Preparation of a new 2D MXene/PES composite membrane with excellent hydrophilicity and high flux, RSC Adv. 7 (2017) 56204–56210.
[22] S. Basu, M. Balakrishnan, Polyamide thin film composite membranes containing ZIF-8 for the separation of pharmaceutical compounds from aqueous streams, Sep. Purif. Technol. 179 (2017) 118–125.
[23] M.S. Denny, J.C. Moreton, L. Benz, S.M. Cohen, Metal-organic frameworks for membrane-based separations, Nat. Rev. Mater. 1 (2016) 16076.
[24] H. Furukawa, K.E. Cordova, M. O'Keeffe, O.M. Yaghi, The chemistry and applications of metal-prganic frameworks, Science 341 (2013) 974.
[25] W.G. Lu, Z.W. Wei, Z.Y. Gu, T.F. Liu, J. Park, J. Park, J. Tian, M.W. Zhang, Q. Zhang, T. Gentle, M. Bosch, H.C. Zhou, Tuning the structure and function of metal-organic frameworks via linker design, Chem. Soc. Rev. 43 (2014) 5561–5593.
[26] J.D. Evans, C.J. Sumby, C.J. Doonan, Post-synthetic metalation of metal-organic frameworks, Chem. Soc. Rev. 43 (2014) 5933–5951.
[27] L. Joseph, B.M. Jun, M. Jang, C.M. Park, J.C. Munoz-Senmache, A.J. Hernandez-Maldonado, A. Heyden, M. Yu, Y. Yoon, Removal of contaminants of emerging concern by metal-organic framework nanoadsorbents: A review, Chem. Eng. J. 369 (2019) 928–946.
[28] B.M. Jun, S. Kim, Y. Kim, N. Her, J. Heo, J. Han, M. Jang, C.M. Park, Y. Yoon, Comprehensive evaluation on removal of lead by graphene oxide and metal organic framework, Chemosphere 231 (2019) 82–92.
[29] B.M. Jun, S. Kim, J. Heo, N. Her, M. Jang, C.M. Park, Y. Yoon, Enhanced sonocatalytic degradation of carbamazepine and salicylic acid using a metal-organic framework, Ultrason. Sonochem. 56 (2019) 174–182.
[30] F. Gholami, S. Zinadini, A.A. Zinatizadeh, A.R. Abbasi, TMU-5 metal-organic frameworks (MOFs) as a novel nanofiller for flux increment and fouling mitigation in PES ultrafiltration membrane, Sep. Purif. Technol. 194 (2018) 272–280.
[31] J. Heo, L.K. Boateng, J.R.V. Flora, H. Lee, N. Her, Y.G. Park, Y. Yoon, Comparison of flux behavior and synthetic organic compound removal by forward osmosis and reverse osmosis membranes, J. Membr. Sci. 443 (2013) 69–82.
[32] M. Arjmandi, M. Peyravi, M.P. Chenar, M. Jahanshahi, A new concept of MOF-based PMM by modification of conventional dense film casting method: Significant impact on the performance of FO process, J. Memb. Sci. 579 (2019) 253–265.
[33] T.Y. Liu, H.G. Yuan, Y.Y. Liu, D. Ren, Y.C. Su, X.L. Wang, Metal-organic framework nanocomposite thin films with interfacial bindings and self-standing robustness for high water flux and enhanced ion selectivity, ACS Nano 12 (2018) 9253–9265.
[34] A. Zirehpour, A. Rahimpour, S. Khoshhal, M.D. Firouzjaei, A.A. Ghoreyshi, The impact of MOF feasibility to improve the desalination performance and antifouling properties of FO membranes, RSC Adv. 6 (2016) 70174–70185.
[35] M. Kadhom, W.M. Hu, B.L. Deng, Thin film nanocomposite membrane filled with metal-organic frameworks UiO-66 and MIL-125 nanoparticles for water desalination, Membranes 7 (2017) 31.
[36] Y. Xu, X.L. Gao, X.J. Wang, Q. Wang, Z.Y. Ji, X.Y. Wang, T. Wu, C.J. Gao, Highly and stably water permeable thin film nanocomposite membranes doped with MIL-101 (Cr) nanoparticles for reverse osmosis application, Materials 9 (2016) 870.
[37] L.Y. Wang, S.X. Duan, M.Q. Fang, J. Liu, J. He, J.D. Li, J.D. Lei, Surface modification route to prepare novel polyamide@NH2_MIL-88B nanocomposite membranes for water treatment, RSC Adv. 6 (2016) 71250–71261.
[38] J.E. Efome, D. Rana, T. Matsuura, C.Q. Lan, Insight studies on metal-organic framework nanofibrous membrane adsorption and activation for heavy metal ions removal from aqueous solution, ACS Appl. Mater. Interfaces 10 (2018) 18619–18629.
[39] Y.R. He, Y.P. Tang, D.C. Ma, T.S. Chung, UiO-66 incorporated thin-film nanocomposite membranes for efficient selenium and arsenic removal, J. Memb. Sci. 541 (2017) 262–270.
[40] M. Navarro, J. Benito, L. Paseta, I. Gascon, J. Coronas, C. Tellez, Thin-film nanocomposite membrane with the minimum amount of MOF by the Langmuir-Schaefer technique for nanofiltration, ACS Appl. Mater. Interfaces 10 (2018) 1278–1287.
[41] H.M. Ruan, C.M. Guo, H.W. Yu, J.N. Shen, C.J. Gao, A. Sotto, B. Van der Bruggen, Fabrication of a MIL-53(Al) nanocomposite membrane and potential application in desalination of dye solutions, Ind. Eng. Chem. Res. 55 (2016) 12099–12110.
[42] J. Ma, X.Y. Guo, Y.P. Ying, D.H. Liu, C.L. Zhong, Composite ultrafiltration membrane tailored by MOF@GO with highly improved water purification performance, Chem. Eng. J. 313 (2017) 890–898.
[43] Z.Y. Ren, J.Q. Luo, Y.H. Wan, Highly permeable biocatalytic membrane prepared by 3D modification: Metal-organic frameworks ameliorate its stability for micropollutants removal, Chem. Eng. J. 348 (2018) 389–398.
[44] Y. Ren, T. Li, W.M. Zhang, S. Wang, M.Q. Shi, C. Shan, W.B. Zhang, X.H. Guan, L. Lv, M. Hua, B.C. Pan, MIL-PVDF blend ultrafiltration membranes with ultrahigh MOF loading for simultaneous adsorption and catalytic oxidation of methylene blue, J. Hazard. Mater. 365 (2019) 312–321.
[45] M. Kadhom, B.L. Deng, Metal-organic frameworks (MOFs) in water filtration membranes for desalination and other applications, Appl. Mater. Today 11 (2018) 219–230.
[46] K.M. Gupta, K. Zhang, J.W. Jiang, Water desalination through zeolitic imidazolate framework membranes: Significant role of functional groups, Langmuir 31 (2015) 13230–13237.
[47] J.Y. Lee, Q.H. She, F.W. Huo, C.Y.Y. Tang, Metal-organic framework-based porous matrix membranes for improving mass transfer in forward osmosis membranes, J. Memb. Sci. 492 (2015) 392–399.
[48] N. Abdullah, M.A. Rahman, M.H.D. Othman, J. Jaafar, A. Abd Aziz, Preparation, characterizations and performance evaluations of alumina hollow fiber membrane incorporated with UiO-66 particles for humic acid removal, J. Memb. Sci. 563 (2018) 162–174.
[49] M. Wu, H.L. Ye, F.Q. Zhao, B.Z. Zeng, High-quality metal-organic framework ZIF-8 membrane supported on electrodeposited ZnO/2-methylimidazole nanocomposite: Efficient adsorbent for the enrichment of acidic drugs, Sci. Rep. 7 (2017) 39778.
[50] Y.C. Liu, M. Zhu, M.Y. Chen, L.L. Ma, B. Yang, L.L. Li, W.W. Tu, A polydopamine-modified reduced graphene oxide (RGO)/MOFs nanocomposite with fast rejection capacity for organic dye, Chem. Eng. J. 359 (2019) 47–57.
[51] M. Wang, X.T. Xu, Y. Liu, Y.J. Li, T. Lu, L.K. Pan, From metal-organic frameworks to porous carbons: A promising strategy to prepare high-performance electrode materials for capacitive deionization, Carbon 108 (2016) 433–439.
[52] E. Elsayed, R. Al-Dadah, S. Mahmoud, P.A. Anderson, A. Elsayed, P.G. Youssef, CPO-27(Ni), aluminium fumarate and MIL-101(Cr) MOF materials for adsorption water desalination, Desalination 406 (2017) 25–36.
[53] J. Zuo, T.S. Chung, Metal-organic framework-functionalized alumina membranes for vacuum membrane distillation, Water 8 (2016) 586.
[54] X. Li, Y.X. Liu, J. Wang, J. Gascon, J.S. Li, B. Van der Bruggen, Metal-organic frameworks based membranes for liquid separation, Chem. Soc. Rev. 46 (2017) 7124–7144.
[55] T.Y. Cath, A.E. Childress, M. Elimelech, Forward osmosis: Principles, applications, and recent developments, J. Memb. Sci. 281 (2006) 70–87.
[56] Y.S. Meng, L. Shu, L. Liu, Y.Q. Wu, L.H. Xie, M.J. Zhao, J.R. Li, A high-flux mixed matrix nanofiltration membrane with highly water-dispersible MOF crystallites as filler, J. Memb. Sci. 591 (2019) 117360.
[57] J.Y. Lee, C.Y.Y. Tang, F.W. Huo, Fabrication of porous matrix membrane (PMM) using metal-organic framework as green template for water treatment, Sci. Rep. 4 (2014) 3740.
[58] O.G. Nik, X.Y. Chen, S. Kaliaguine, Functionalized metal organic framework-polyimide mixed matrix membranes for CO2/CH4 separation, J. Memb. Sci. 413 (2012) 48–61.
[59] R.B. Dai, X.R. Zhang, M.X. Liu, Z.C. Wu, Z.W. Wang, Porous metal organic framework CuBDC nanosheet incorporated thin-film nanocomposite membrane for high-performance forward osmosis, J. Memb. Sci. 573 (2019) 46–54.
[60] M. Kim, J.F. Cahill, H.H. Fei, K.A. Prather, S.M. Cohen, Postsynthetic ligand and cation exchange in robust metal-organic frameworks, J. Am. Chem. Soc. 134 (2012) 18082–18088.
[61] H.G. Yuan, Y.Y. Liu, T.Y. Liu, X.L. Wang, Self-standing nanofilms of polysulfone doped with sulfonated polysulfone via solvent evaporation for forward osmosis, J. Memb. Sci. 523 (2017) 567–575.
[62] J. Ren, M.R. Chowdhury, J. Qi, L.L. Xia, B.D. Huey, J.R. McCutcheon, Relating osmotic performance of thin film composite hollow fiber membranes to support layer surface pore size, J. Memb. Sci. 540 (2017) 344–353.
[63] S. Samarasinghe, C.Y. Chuah, Y.Q. Yang, T.H. Bae, Tailoring CO2/CH4 separation properties of mixed-matrix membranes via combined use of two- and three-dimensional metal-organic frameworks, J. Memb. Sci. 557 (2018) 30–37.
[64] S.J. Kim, S. Kook, B.E. O'Rourke, J. Lee, M. Hwang, Y. Kobayashi, R. Suzuki, I.S. Kim, Characterization of pore size distribution (PSD) in cellulose triacetate (CTA) and polyamide (PA) thin active layers by positron annihilation lifetime spectroscopy (PALS) and fractional rejection (FR) method, J. Memb. Sci. 527 (2017) 143–151.
[65] L. Shen, S. Xiong, Y. Wang, Graphene oxide incorporated thin-film composite membranes for forward osmosis applications, Chem. Eng. Sci. 143 (2016) 194–205.
[66] A.C. Elder, A.B. Aleksandrov, S. Nair, T.M. Orlando, Interactions on external MOF surfaces: Desorption of water and ethanol from CuBDC nanosheets, Langmuir 33 (2017) 10153–10160.
[67] S.J. You, C.Y. Tang, C. Yu, X.H. Wang, J.N. Zhang, J. Han, Y. Gan, N.Q. Ren, Forward osmosis with a novel thin-film inorganic membrane, Environ. Sci. Technol. 47 (2013) 8733–8742.
[68] S. Turgman-Cohen, J.C. Araque, E.M.V. Hoek, F.A. Escobedo, Molecular dynamics of equilibrium and pressure-driven transport properties of water through LTA-type zeolites, Langmuir 29 (2013) 12389–12399.

[69] S.F. Seyedpour, A. Rahimpour, A.A. Shamsabadi, M. Soroush, Improved performance and antifouling properties of thin-film composite polyamide membranes modified with nano-sized bactericidal graphene quantum dots for forward osmosis, Chem. Eng. Res. Des. 139 (2018) 321–334.
[70] M.D. Firouzjaei, A.A. Shamsabadi, S.A. Aktij, S.F. Seyedfour, M. Sharifian Gh, A. Rahimpour, M.R. Esfahani, M. Ulbricht, M. Soroush, Exploiting synergetic effects of graphene oxide and a silver-based metal-organic framework to enhance antifouling and anti-biofouling properties of thin-film nanocomposite membranes, ACS Appl. Mater. Interfaces 10 (2018) 42967–42978.
[71] M.D. Firouzjaei, A.A. Shamsabadi, M.S. Gh, A. Rahimpour, M. Soroush, A novel nanocomposite with superior antibacterial activity: A silver-based metal organic framework embellished with graphene oxide, Adv. Mater. Interfaces 5 (2018) 1701365.
[72] J. Wei, C.Q. Qiu, C.Y.Y. Tang, R. Wang, A.G. Fane, Synthesis and characterization of flat-sheet thin film composite forward osmosis membranes, J. Memb. Sci. 372 (2011) 292–302.
[73] Y. Xu, X.Y. Peng, C.Y.Y. Tang, Q.S.A. Fu, S.Z. Nie, Effect of draw solution concentration and operating conditions on forward osmosis and pressure retarded osmosis performance in a spiral wound module, J. Memb. Sci. 348 (2010) 298–309.
[74] D.C. Ma, S.B. Peh, G. Han, S.B. Chen, Thin-film nanocomposite (TFN) membranes incorporated with super-hydrophilic metal-organic framework (MOF) UiO-66: Toward enhancement of water flux and salt rejection, ACS Appl. Mater. Interfaces 9 (2017) 7523–7534.
[75] J. Pang, Z.X. Kang, R.M. Wang, B. Xu, X.Y. Nie, L.L. Fan, F.X. Zhang, X.X. Du, S. Feng, D.F. Sun, Exploring the sandwich antibacterial membranes based on UiO-66/graphene oxide for forward osmosis performance, Carbon 144 (2019) 321–332.
[76] M. Qiu, C.J. He, Efficient removal of heavy metal ions by forward osmosis membrane with a polydopamine modified zeolitic imidazolate framework incorporated selective layer, J. Hazard. Mater. 367 (2019) 339–347.
[77] R.J. Petersen, Composite reverse-osmosis and nanofiltration membranes, J. Memb. Sci. 83 (1993) 81–150.
[78] J.T. Duan, Y.C. Pan, F. Pacheco, E. Litwiller, Z.P. Lai, I. Pinnau, High-performance polyamide thin-film-nanocomposite reverse osmosis membranes containing hydrophobic zeolitic imidazolate framework-8, J. Memb. Sci. 476 (2015) 303–310.
[79] H.M. Park, K.Y. Jee, Y.T. Lee, Preparation and characterization of a thin-film composite reverse osmosis membrane using a polysulfone membrane including metal-organic frameworks, J. Memb. Sci. 541 (2017) 510–518.
[80] P.K. Samantaray, G. Madras, S. Bose, Water remediation aided by a graphene-oxide-anchored metal organic framework through pore- and charge-based sieving of ions, ACS Sustain. Chem. Eng. 7 (2019) 1580–1590.
[81] H. Huang, X.Y. Qu, X.S. Ji, X. Gao, L. Zhang, H.L. Chen, L. Hou, Acid and multivalent ion resistance of thin film nanocomposite RO membranes loaded with silicalite-1 nanozeolites, J. Mater. Chem. A 1 (2013) 11343–11349.
[82] L. Zhang, G.Z. Shi, S. Qiu, L.H. Cheng, H.L. Chen, Preparation of high-flux thin film nanocomposite reverse osmosis membranes by incorporating functionalized multi-walled carbon nanotubes, Desalin. Water Treat. 34 (2011) 19–24.
[83] Z.Q. Hu, Y.F. Chen, J.W. Jiang, Zeolitic imidazolate framework-8 as a reverse osmosis membrane for water desalination: Insight from molecular simulation, J. Chem. Phys. 134 (2011).
[84] J.J. Gutierrez-Sevillano, D. Dubbeldam, L. Bellarosa, N. Lopez, X. Liu, T.J.H. Vlugt, S. Calero, Strategies to simultaneously enhance the hydrostability and the alcohol-water separation behavior of Cu-BTC, J. Phys. Chem. C 117 (2013) 20706–20714.
[85] E.R. Nightingale, Phenomenological theory of ion solvation-Effective radii of hydrated ions, J. Phys. Chem. 63 (1959) 1381–1387.
[86] J. Yin, E.S. Kim, J. Yang, B.L. Deng, Fabrication of a novel thin-film nanocomposite (TFN) membrane containing MCM-41 silica nanoparticles (NPs) for water purification, J. Memb. Sci. 423 (2012) 238–246.
[87] M. Fathizadeh, A. Aroujalian, A. Raisi, Effect of lag time in interfacial polymerization on polyamide composite membrane with different hydrophilic sub layers, Desalination 284 (2012) 32–41.
[88] L.Y. Wang, M.Q. Fang, J. Liu, J. He, J.D. Li, J.D. Lei, Layer-by-layer fabrication of high-performance polyamide/ZIF-8 nanocomposite membrane for nanofiltration applications, ACS Appl. Mater. Interfaces 7 (2015) 24082–24093.
[89] P. Marchetti, M. Mechelhoff, A.G. Livingston, Tunable-porosity membranes from discrete nanoparticles, Sci. Rep. 5 (2015) 17353.
[90] X.Q. Cheng, S.G. Ding, J. Guo, C. Zhang, Z.H. Guo, L. Shao, In-situ interfacial formation of TiO2/polypyrrole selective layer for improving the separation efficiency towards molecular separation, J. Memb. Sci. 536 (2017) 19–27.
[91] X.Q. Cheng, X. Jiang, Y.Q. Zhang, C.H. Lau, Z.L. Xie, D. Ng, S.J.D. Smith, M.R. Hill, L. Shao, Building additional passageways in polyamide membranes with hydrostable metal organic frameworks to recycle and remove organic solutes from various solvents, ACS Appl. Mater. Interfaces 9 (2017) 38877–38886.
[92] G. Gnanasekaran, S. Balaguru, G. Arthanareeswaran, D.B. Das, Removal of hazardous material from wastewater by using metal organic framework (MOF) embeddedpolymeric membranes, Sep. Purif. Technol. 54 (2019) 434–446.
[93] Z. Rao, K. Feng, B.B. Tang, P.Y. Wu, Surface decoration of amino-functionalized metal organic framework/graphene oxide composite onto polydopamine-coated membrane substrate for highly efficient heavy metal removal, ACS Appl. Mater. Interfaces 9 (2017) 2594–2605.
[94] Z.P. Liao, X.F. Fang, J. Xie, Q. Li, D.P. Wang, X.Y. Sun, L.J. Wang, J.S. Li, Hydrophilic hollow nanocube-functionalized thin film nanocomposite membrane with enhanced nanofiltration performance, ACS Appl. Mater. Interfaces 11 (2019) 5344–5352.
[95] H.Q. Wu, Y.J. Liu, L. Mao, C.H. Jiang, J.M. Ang, X.H. Lu, Doping polysulfone ultrafiltration membrane with TiO2-PDA nanohybrid for simultaneous self-cleaning and self-protection, J. Memb. Sci. 532 (2017) 20–29.
[96] L. Paseta, D. Antoran, J. Coronas, C. Tellez, 110th anniversary: polyamide/metal-organic framework bilayered thin film composite membranes for the removal of pharmaceutical compounds from water, Ind. Eng. Chem. Res. 58 (2019) 4222–4230.
[97] H.Y. Yang, N.X. Wang, L. Wang, H.X. Liu, Q.F. An, S.L. Ji, Vacuum-assisted assembly of ZIF-8@GO composite membranes on ceramic tube with enhanced organic solvent nanofiltration performance, J. Memb. Sci. 545 (2018) 158–166.
[98] Z.G. Hu, Y.W. Peng, Z.X. Kang, Y.H. Qian, D. Zhao, A Modulated Hydrothermal (MHT) Approach for the Facile Synthesis of UiO66-Type MOFs, Inorg. Chem. 54 (2015) 4862–4868.
[99] P. Vandezande, L.E.M. Gevers, I.F.J. Vankelecom, Solvent resistant nanofiltration: separating on a molecular level, Chem. Soc. Rev. 37 (2008) 365–405.
[100] S.J.D. Smith, B.P. Ladewig, A.J. Hill, C.H. Lau, M.R. Hill, Post-synthetic Ti exchanged UiO-66 metal-organic frameworks that deliver exceptional gas permeability in mixed matrix membranes, Sci. Rep. 5 (2015) 7823.
[101] G. Rodrigues, D.S. Monteiro, C.D. Meireles, R.M.N. de Assuncao, D.A. Cerqueira, H.S. Barud, S.J.L. Ribeiro, Y. Messadeq, Synthesis and characterization of cellulose acetate produced from recycled newspaper, Carbohyd. Polym. 73 (2008) 74–82.
[102] N. Nikooe, E. Saljoughi, Preparation and characterization of novel PVDF nanofiltration membranes with hydrophilic property for filtration of dye aqueous solution, Appl. Surf. Sci. 413 (2017) 41–49.
[103] G.P. Wu, S.Y. Gan, L.Z. Cui, Y.Y. Xu, Preparation and characterization of PES/TiO2 composite membranes, Appl. Surf. Sci. 254 (2008) 7080–7086.
[104] K. Ohwada, On the Pauling electronegativity scales, Polyhedron 2 (1983) 423–424.
[105] A.B. Holmes, F.X. Gu, Emerging nanomaterials for the application of selenium removal for wastewater treatment, Environ. Sci. Nano 3 (2016) 982–996.
[106] Y.L. Ji, Q.F. An, Y.S. Guo, W.S. Hung, K.R. Lee, C.J. Gao, Bio-inspired fabrication of high perm-selectivity and anti-fouling membranes based on zwitterionic polyelectrolyte nanoparticles, J. Mater. Chem. A 4 (2016) 4224–4231.
[107] X.R. Hu, C.H. Wang, J.S. Li, R. Luo, C. Liu, X.Y. Sun, J.Y. Shen, W.Q. Han, L.J. Wang, Metal organic framework-derived hollow carbon nanocubes for fast solid-phase microextraction of polycyclic aromatic hydrocarbons, ACS Appl. Mater. Interfaces 10 (2018) 15051–15057.
[108] H.Z. Sun, P.Y. Wu, Tuning the functional groups of carbon quantum dots in thin film nanocomposite membranes for nanofiltration, J. Memb. Sci. 564 (2018) 394–403.
[109] A. Rahimpour, S.F. Seyedpour, S.A. Aktij, M.D. Firouzjaei, A. Zirehpour, A.A. Shamsabadi, S.K. Salestan, M. Jabbari, M. Soroush, Simultaneous improvement of antimicrobial, antifouling, and transport properties of forward osmosis membranes with immobilized highly-compatible polyrhodanine nanoparticles, Environ. Sci. Technol. 52 (2018) 5246–5258.
[110] M. Safarpour, V. Vatanpour, A. Khataee, Preparation and characterization of graphene oxide/TiO2 blended PES nanofiltration membrane with improved antifouling and separation performance, Desalination 393 (2016) 65–78.
[111] A.D. Marshall, P.A. Munro, G. Tragardh, The effect of protein fouling in microfiltration and ultrafiltration on permeate flux, protein retention and selectivity - A literature review, Desalination 91 (1993) 65–108.
[112] X.L. Liu, N.K. Demir, Z.T. Wu, K. Li, Highly water-stable zirconium metal organic framework UiO-66 membranes supported on alumina hollow fibers for desalination, J. Am. Chem. Soc. 137 (2015) 6999–7002.
[113] T. Li, W.M. Zhang, S. Zhai, G.D. Gao, J. Ding, W.B. Zhang, Y. Liu, X. Zhao, B.C. Pan, L. Lv, Efficient removal of nickel(II) from high salinity wastewater by a novel PAA/ZIF-8/PVDF hybrid ultrafiltration membrane, Water Res. 143 (2018) 87–98.
[114] T.A. Makhetha, R.M. Moutloali, Antifouling properties of Cu(tpa)@GO/PES composite membranes and selective dye rejection, J. Memb. Sci. 554 (2018) 195–210.
[115] H.Z. Sun, B.B. Tang, P.Y. Wu, Development of hybrid ultrafiltration membranes with improved water separation properties using modified superhydrophilic metal-organic framework nanoparticles, ACS Appl. Mater. Interfaces 9 (2017) 21473–21484.
[116] J.A. Prince, S. Bhuvana, V. Anbharasi, N. Ayyanar, K.V.K. Boodhoo, G. Singh, Self-cleaning metal organic framework (MOF) based ultra filtration membranes A solution to bio-fouling in membrane separation processes, Sci. Rep. 4 (2014) 6555.
[117] F. Zhang, W.B. Zhang, Y. Yu, B. Deng, J.Y. Li, J. Jin, Sol-gel preparation of PAA-g-PVDF/TiO2 nanocomposite hollow fiber membranes with extremely high water flux and improved antifouling property, J. Memb. Sci. 432 (2013) 25–32.
[118] H.Z. Sun, B.B. Tang, P.Y. Wu, Hydrophilic hollow zeolitic imidazolate framework-8 modified ultrafiltration membranes with significantly enhanced water separation properties, J. Memb. Sci. 551 (2018) 283–293.
[119] Z.W. Xu, J.G. Zhang, M.J. Shan, Y.L. Li, B.D. Li, J.R. Niu, B.M. Zhou, X.M. Qian, Organosilane-functionalized graphene oxide for enhanced antifouling and mechanical properties of polyvinylidene fluoride ultrafiltration membranes, J. Memb. Sci. 458 (2014) 1–13.
[120] Y.N. Yang, H.X. Zhang, P. Wang, Q.Z. Zheng, J. Li, The influence of nano-sized TiO2 fillers on the morphologies and properties of PSFUF membrane, J. Memb. Sci. 288 (2007) 231–238.
[121] W. Yuan, A.L. Zydney, Humic acid fouling during ultrafiltration, Environ. Sci. Technol. 34 (2000) 5043–5050.
[122] A. Rahimpour, M. Jahanshahi, S. Khalili, A. Mollahosseini, A. Zirepour, B. Rajaeian, Novel functionalized carbon nanotubes for improving the surface properties and performance of polyethersulfone (PES) membrane, Desalination 286 (2012) 99–107.

[123] H. Salehi, A. Shakeri, H. Naslhajian, M. Amini, High-flux thin film nanocomposite forward osmosis membrane incorporated with blue lemon polyoxometalate based open-framework, J. Polym. Res. 26 (2019).
[124] S.F. Seyedpour, A. Rahimpour, G. Najafpour, Facile in-situ assembly of silver-based MOFs to surface functionalization of TFC membrane: A novel approach toward long-lasting biofouling mitigation, J. Memb. Sci. 573 (2019) 257–269.
[125] A. Zirehpour, A. Rahimpour, M. Ulbricht, Nano-sized metal organic framework to improve the structural properties and desalination performance of thin film composite forward osmosis membrane, J. Memb. Sci. 531 (2017) 59–67.
[126] E.S. Mansor, T.S. Jamil, H. Abdallah, A.M. Shaban, Highly thin film nanocomposite membrane based metal organic complexes for brackish water desalination, J. Environ. Chem. Eng. 6 (2018) 5459–5469.
[127] Y. Li, L.H. Wee, J.A. Martens, I.F.J. Vankelecom, Interfacial synthesis of ZIF-8 membranes with improved nanofiltration performance, J. Memb. Sci. 523 (2017) 561–566.
[128] F. Mohammadnezhad, M. Feyzi, S. Zinadini, A novel Ce-MOF/PES mixed matrix membrane; synthesis, characterization and antifouling evaluation, J. Ind. Eng. Chem. 71 (2019) 99–111.
[129] S.J. Yang, Q.F. Zou, T.H. Wang, L.P. Zhang, Effects of GO and MOF@GO on the permeation and antifouling properties of cellulose acetate ultrafiltration membrane, J. Memb. Sci. 569 (2019) 48–59.
[130] N. Yin, K. Wang, L.Z. Wang, Z.Q. Li, Amino-functionalized MOFs combining ceramic membrane ultrafiltration for Pb (II) removal, Chem. Eng. J. 306 (2016) 619–628.